Prosapip1 in the dorsal hippocampus mediates synaptic protein composition, long-term potentiation, and spatial memory

Zachary W. Hoisington[1], Himanshu Gangal[2], Khanhky Phamluong[1], Chhavi Shukla[1], Yann Ehinger[1], Jeffrey J. Moffat[1], Gregg E. Homanics[3], Jun Wang[2], and Dorit Ron[1]

[1]Alcohol and Addiction Research Group, Department of Neurology, University of California San Francisco; [2]Department of Neuroscience and Experimental Therapeutics, School of Medicine, Texas A&M University Health Science Center; [3]Department of Anesthesiology and Perioperative Medicine, University of Pittsburgh

*Correspondence: D. Ron, Department of Neurology, University of California, San Francisco, 675 Nelson Rising Lane, BOX 0663, San Francisco, CA, USA. dorit.ron@ucsf.edu

Abstract

Prosapip1 is a brain-specific protein localized to the postsynaptic density, where it promotes dendritic spine maturation in primary hippocampal neurons. However, nothing is known about the role of Prosapip1 *in vivo*. To examine this, we utilized the Cre-loxP system to develop a Prosapip1 neuronal knockout mouse. We found that Prosapip1 controls the synaptic localization of its binding partner SPAR, along with PSD-95 and the GluN2B subunit of the NMDA receptor (NMDAR) in the dorsal hippocampus (dHP). We next sought to identify the potential contribution of Prosapip1 to the activity and function of the NMDAR and found that Prosapip1 plays an important role in NMDAR-mediated transmission and long-term potentiation (LTP) in the CA1 region of the dHP. As LTP is the cellular hallmark of learning and memory, we examined the consequences of neuronal knockout of Prosapip1 on dHP-dependent memory. We found that global or dHP-specific neuronal knockout of Prosapip1 caused a deficit in learning and memory whereas developmental, locomotor, and anxiety phenotypes were normal. Taken together, Prosapip1 in the dHP promotes the proper localization of synaptic proteins which, in turn, facilitates LTP driving recognition, social, and spatial learning and memory.

30 **Introduction**

31 ProSAP-interacting protein 1 (Prosapip1), encoded by the gene *LZTS3*, is a brain-specific
32 protein that shows particularly high expression in the cortex, cerebellum, and hippocampus
33 (Wendholt et al., 2006; Laguesse et al., 2017). Prosapip1 is highly enriched in the PSD of
34 excitatory synapses and plays an important role in dendritic spine maturation in primary
35 hippocampal neurons (Wendholt et al., 2006; Dolnik et al., 2016). The PSD is a complex protein
36 network located at the postsynaptic membrane of neurons, namely excitatory neurons (Boeckers
37 et al., 2002; Kaizuka and Takumi, 2018). The PSD is crucial for synaptic transmission and
38 plasticity (Boeckers et al., 2002; Kaizuka and Takumi, 2018), and abnormalities in the PSD
39 network are linked to various neuropsychiatric and neurodegenerative disorders (Kaizuka and
40 Takumi, 2018), such as schizophrenia, autism spectrum disorder (ASD), depression, and
41 Alzheimer's disease (Kaizuka and Takumi, 2018). The PSD contains scaffolding proteins such as
42 PSD-95, Shank, and Homer (Kennedy, 2018). The major scaffold in the PSD is actin (Qualmann
43 et al., 2004), which recycles between globular (G-actin) and filamentous (F-actin), and is crucial
44 in reorganizing and stabilizing the PSD (Qualmann et al., 2004; Kuriu et al., 2006).

45 Prosapip1 has a C-terminal Fez1 domain that it shares with the other members of the
46 Fezzin family (LAPSER1, PSD-Zip70, N4BP3) (Wendholt et al., 2006). Fezzins interact with the
47 PDZ (PSD-95/Dlg1/ZO-1) domain of SH3 and multiple ankyrin repeat domains (Shank) family
48 proteins. Shanks are also known as proline-rich synapse-associated proteins (ProSAPs) and
49 were originally identified as proteins primarily localizing in the PSD of excitatory synapses
50 (Boeckers et al., 1999; Sheng and Kim, 2000; Boeckers et al., 2002). Prosapip1 specifically
51 interacts with the PSD protein, Shank3 (Wendholt et al., 2006). Prosapip1 also interreacts with
52 the spine-associated Rap GTPase-activating protein (SPAR) (Wendholt et al., 2006; Reim et al.,
53 2016). SPAR catalyzes the conversion of the small G-protein Rap from its active, GTP-bound
54 form to its inactive GDP-bound form, thereby inhibiting Rap activity. SPAR is an essential
55 modulator of spine morphology through its interaction with actin (Pak et al., 2001; Richter et al.,

56 2007). In hippocampal neurons, it is localized to dendritic spines and leads to spine head
57 enlargement (Pak et al., 2001). SPAR also associates with PSD-95/NMDAR-complex
58 components (Matsuura et al., 2022). Wendholt et al reported that in primary hippocampal neurons
59 Prosapip1 regulates the synaptic levels of SPAR by scaffolding it to Shank3 (Wendholt et al.,
60 2006; Dolnik et al., 2016; Reim et al., 2016).

61 We previously found that *Prosapip1* mRNA to protein translation is controlled by the
62 mechanistic target of rapamycin complex 1 (mTORC1) in the nucleus accumbens (NAc) of mice
63 consuming large quantities of alcohol (Laguesse et al., 2017). We further showed that Prosapip1
64 interacts with SPAR in the NAc and leads to alcohol-dependent synaptic and structural plasticity
65 (Laguesse et al., 2017). Specifically, we found that knockdown of Prosapip1 in the NAc led to a
66 reduction in F-actin, while overexpression of Prosapip1 led to an increase in F-actin (Laguesse et
67 al., 2017). Knockdown of Prosapip1 led to a reduction of mature, mushroom-type spines and an
68 increase in immature, thin spines (Laguesse et al., 2017). Finally, we found that Prosapip1 in the
69 NAc contributes to alcohol self-administration and reward (Laguesse et al., 2017). However,
70 nothing is known about the normal *in vivo* role of Prosapip1 in the central nervous system (CNS).
71 Here, we report that Prosapip1 in the dorsal hippocampus (dHP) controls the localization of
72 synaptic proteins at the PSD and contributes to long-term potentiation (LTP) as well as
73 recognition, social, and spatial learning and memory.

Materials and Methods

Animals

Prosapip1(flx/flx) mice were generated as described below. Syn1-Cre(+) mice were purchased from Jackson Laboratory (Stock #003966, Bar Harbor, Maine). Prosapip1(flx/flx) and Prosapip1(flx/flx);Syn1-Cre mice were bred and group housed in a 12-hour light-dark cycle room that was temperature- and humidity-controlled. Unrestricted amounts of food and water were provided. Animal procedures were approved by the UCSF Institutional Animal Care and Use Committee (IACUC).

Generation of Prosapip1 Floxed Mice

Guide RNA binding sites in intron 2 and in the 3'UTR located in Exon 5 of Prosapip1 (a.k.a, *Lzts3*) (**Figure 1A**) were identified using the CRISPRator tool (Labuhn et al., 2018) within the CCTop (Stemmer et al., 2015) online platform (http://crispr.cos.uni-heidelberg.de/). The gRNA binding sites are located ~3.3kb from each other. These gRNA target sites were used to produce two Alt-R CRISPR-Cas9 crRNAs (IDT DNA, Coralville, IA) which were individually hybridized to a universal 67-mer Alt-R CRISPR-Cas9 tracrRNA (IDT DNA) to produce two gRNAs. Two 140 nt long PAGE purified Ultramer single stranded DNA Oligos (IDT DNA) with three phosphorotioate modifications on each end (Renaud et al., 2016) that were homologous to the target loci in intron 2 and Exon 5 (**Figure 1B**) were used as a repair templates.

We introduced each loxP site into 1-cell and 2-cell stages of embryonic development (Horii et al., 2017). Single cell C57BL/6J embryos were electroporated with gRNA#6 (200ng/µl), IDT Alt-R® HiFi Cas9 Nuclease V3 protein (75ng/µl), and Exon 5 repair template (200ng/µl) using a BioRad Gene-Pulser Xcell electroporator in a 1 mm-gap slide electrode (Protech International, #501P1-10) using square-wave pulses (five repeats of 3 msec 25V pulses with 100 ms interpulse intervals). Following this first electroporation, embryos were cultured overnight. Surviving two-cell embryos were electroporated with gRNA#7 (200ng/µl), IDT Alt-R® HiFi Cas9 Nuclease V3 protein

100 (75ng/µl), and intron 2 repair template (200ng/µl) under conditions described above. Surviving
101 embryos were transferred to the oviducts of CD1 (Charles River) pseudopregnant recipient
102 females. Offspring were genotyped for the intron 2 lox insertion using PCR (forward primer 5'
103 AGAGAAGTCTACGCTGTAGTCAG 3' and reverse primer 5' AAGCGGGAAGGTAGAGAGGT 3';
104 wild type product = 449bp, floxed product = 489bp) followed by Sanger sequencing. Offspring
105 were genotyped for the Exon 5 lox insertion using PCR (forward primer 5'
106 TGCACAACCTTCTGACACGT 3' and reverse primer 5' AGGGCACAGACAGTAGCACT 3'; wild
107 type product = 408bp, floxed product = 448bp) followed by Sanger sequencing. Two founder
108 animals were found that harbored loxP insertions at both the intron 2 and Exon 5 sites. When
109 mated to C57BL/6J females, the loxP sites segregated indicating that they were on different
110 chromosomes. Therefore, F1 offspring that harbored only the loxP insertion at the intron 2 site
111 were used as 1-cell embryo donors for insertion of the Exon 5 loxP site using electroporation
112 conditions described above. One male offspring was produced that harbored both the intron 2
113 and Exon 5 loxP insertions on the same chromosome. This male was mated to C57BL/6J females
114 to establish the floxed mouse line used here.
115 Guide RNA off target sites were predicted and ranked using CRISPOR (Concordet and
116 Haeussler, 2018). The top 11 and 10 sites for gRNA#6 and gRNA#7, respectively based on CFD
117 score were amplified from this founder mouse DNA and Sanger sequenced. All predicted off
118 target sites analyzed were wild type (data not shown).
119
120 **Reagents**
121 Antibodies: Rabbit anti-SPAR (SIPA1L1) (1:500) (25086-1-AP) antibodies were purchased from
122 ProteinTech. Mouse anti-Shank3 antibodies (1:500) (#ab93607) were purchased from Abcam.
123 Rabbit anti-GluN2B (1:1000) (#4212), Rabbit anti-GluA1 (1:1000) (#13185S), and Rabbit anti-
124 CREB (1:500) (#9197) antibodies were purchased from Cell Signaling. Goat anti-GluN2A
125 antibodies (1:500) (#SC-1468) were purchased from Santa Cruz. Mouse anti-GAPDH antibodies

126 (1:10,000) (#G8795) were purchased from Sigma. Mouse anti-PSD-95 antibodies (1:100,000)
127 (#05-494) were purchased from Millipore (Upstate). Donkey anti-rabbit horseradish peroxidase
128 (HRP), donkey anti-goat HRP, and donkey anti-mouse HRP conjugated secondary antibodies
129 (1:5000) were purchased from Jackson ImmunoResearch (West Grove, PA). Enhance
130 Chemiluminescence reagent (ECL) was purchased from Millipore (Burlington, MA). EDTA-free
131 complete mini–Protease Inhibitor Cocktails was from Roche (Indianapolis, IN). Pierce
132 bicinchoninic acid (BCA) protein assay kit was purchased from Thermo Scientific (Rockford, IL).
133 NuPAGE Bis-Tris precast gels were purchased from Life Technologies (Carlsbad, CA).
134 Viruses: AAV8-Ef1a-mCherry-IRES-Cre ($1x10^{13}$ vg/ml #55632) and AAV2-CMV-EGFP ($1x10^{13}$
135 vg/ml, #105530) were purchased from Addgene.
136
137 **Crude synaptosomal fractionation**
138 Tissue was first homogenized at 4°C in 500 µl of Krebs buffer including 125 mM NaCl, 1.2 mM
139 KCl, 1.2 mM $MgSO_4$, 1.2 mM $CaCl_2$, 22 mM Na_2CO_3, 1 mM NaH_2PO_4, 10 mM Glucose, 0.32 M
140 sucrose and protease/phosphatase inhibitors. A portion of the homogenate (100 µl) was saved
141 as total homogenate (H), while the remaining homogenate was diluted by adding 500 µl of Krebs
142 buffer to the remaining 400 µl. The total homogenate was transferred to a 1.5 ml Eppendorf tube.
143 The glass homogenizer was washed with 500 µl of Krebs buffer, and the wash solution was added
144 to the remaining homogenate. The sample was then centrifuged at 1,000g at 4°C for 10 minutes.
145 The supernatant (S1) was collected. The process was repeated, and then the S1 supernatant
146 was centrifuged at 16,000g at 4°C for 20 min. The supernatant (S2) was saved, and the pellet
147 was kept on ice. The resulting pellet contained the synaptosomal fraction. The pellet was then
148 resuspended in 500 ul of Krebs buffer and centrifuged at 16,000g 4°C for 20 minutes and
149 resuspended in radio immunoprecipitation assay (RIPA) buffer (containing 50 mM Tris-HCL, 5

150 mM EDTA, 120 mM NaCl, 1%NP-40, 0.1% deoxycholate, 0.5% SDS, and protease and
151 phosphatase inhibitors) for analysis.
152
153 **Western blot analysis**
154 Tissue collected from mice was homogenized in ice-cold RIPA buffer using a sonic dismembrator.
155 Protein concentration was determined using the BCA™ protein assay kit. 30 µg of each tissue
156 lysate was loaded for separation by SDS-PAGE (4-12%), followed by transfer onto a nitrocellulose
157 membrane at 300mA for 2 hours. The membranes were then blocked with 5% milk-PBS
158 containing 0.1% Tween 20 at room temperature for 30 minutes before being probed with the
159 appropriate primary antibodies overnight at 4ºC. Following washing, the membranes were
160 incubated with HRP-conjugated secondary antibodies for one hour at room temperature and then
161 visualized using ECL. Band intensities were quantified using ImageJ software (NIH,
162 https://imagej.net/ij/).
163
164 **Electrophysiology**
165 **Preparation of slices** is outlined in (Gangal et al., 2023). In brief, coronal sections of the
166 hippocampus (250 µm) were cut in an ice-cold solution containing the following: 40 mM NaCl,
167 148.5 mM sucrose, 4.5 mM KCl, 1.25 mM NaH_2PO_4, 25 mM $NaHCO_3$, 0.5 mM $CaCl_2$, 7 mM
168 $MgSO_4$, 10 mM dextrose, 1 mM sodium ascorbate, 3 mM myo-inositol, 3 mM sodium pyruvate
169 and saturated with a 95% O_2 and 5% CO_2. After cutting, the slices were incubated for 45 minutes
170 in an external solution containing the following: 125 mM NaCl, 4.5 mM KCl, 2.5 mM $CaCl_2$, 1.3
171 mM $MgSO_4$, 1.25 mM NaH_2PO_4, 25 mM $NaHCO_3$, 15 mM sucrose, 15 mM glucose and saturated
172 with 95% O_2 and 5% CO_2.
173 **Field potential recordings** were conducted as detailed in previous studies (Wang et al.,
174 2012)**.** Specifically, the procedure involved the use of stimulation electrodes filled with artificial
175 cerebrospinal fluid (aCSF) and placed in the CA1 region of the dHP. The recording electrode,

176 filled with 1M NaCl, was positioned in the CA1 region, approximately 100-150 μm away from the
177 stimulating electrodes. The optimal location for the recording electrode was determined based on
178 the site where a stable fiber volley and field potential response could be consistently observed
179 following the delivery of a single electrical stimulation pulse (2 ms). The stimulation intensity was
180 carefully adjusted to elicit 50% of the maximum possible response. Baseline field potentials were
181 meticulously recorded over 10 mins at 10-second intervals. The HFS protocol for LTP included a
182 regimen of 100 Hz, with 100 pulses every 20 seconds, repeated four times. Following the HFS
183 protocol, field potential recordings were extended for 30 min. LTP was quantified based on the
184 averaged fEPSP as a percentage of the baseline, comparing the measurements at 20-30 minutes
185 post-HFS between the Prosapip1(flx/flx);Syn1-Cre(-) and Prosapip1(flx/flx);Syn1-Cre(+) groups.
186 To inhibit GABAergic transmission, picrotoxin (100 μM) was applied to the bath. The
187 measurement of fEPSP was performed using a MultiClamp 700B amplifier integrated with
188 Clampex 10.4 software provided by Molecular Devices.

189 **Whole-cell recordings** were executed following the protocols previously established
190 (Wang et al., 2012; Ma et al., 2018). For these recordings, a cesium-based intracellular solution
191 was employed. This solution comprised of the following components 119 mM $CsMeSO_4$, 8 mM
192 Tetraethylammonium chloride (TEA-Cl), 15 mM HEPES, 0.6 mM ethylene glycol tetraacetic acid
193 (EGTA), 0.3 mM Na_3GTP, 4 mM MgATP, 5 mM QX-314-Cl, and 7 mM phosphocreatine. The pH
194 of this solution was adjusted to 7.3 using CsOH. The temperature of the recording bath was
195 maintained at a constant 32°C, and the perfusion speed was set between 2-3 ml/min. For the
196 recordings, CA1 neurons were voltage-clamped at a holding potential of -70 mV. In order to
197 measure NMDAR-mediated transmission, a low external concentration of Mg^{2+} (0.05 mM) was
198 used. This was coupled with NBQX (10 μM) and picrotoxin (100 μM) to block AMPA receptor
199 (AMPAR)-mediated synaptic transmission and inhibitory synaptic currents. NMDA-induced
200 currents were measured by bath-applying NMDA (20 μM) for 30 seconds, with holding currents
201 recorded every 5 seconds.

202 **Input-output curves** for NMDAR-mediated EPSC were created by electrical stimulation
203 of varying intensities which were delivered through electrodes strategically placed within the CA1
204 region. The paired-pulse ratio (PPR) was calculated by dividing the amplitude of the second
205 electrically-evoked EPSC by that of the first, with an interval of 100 ms between the two pulses.
206 Additionally, gap-free recordings of spontaneous excitatory postsynaptic currents were conducted
207 over a duration of 2 minutes.
208
209 **Behavior**
210 All behavioral paradigms were completed between the hours of 9:00 and 18:00. Mice were
211 tested between 8 and 20 weeks of age and were age-matched based on experiment. The mice
212 were moved from their housing room, currently in the “light cycle,” to the dimly lit behavior room
213 (10-15 lux) 30 minutes before the experiment and allowed to acclimate. The light/dark box,
214 elevated plus maze, and Barnes maze experiments were done in full room light. During
215 experiments, white noise was played through a speaker in the room at 50dB to reduce influence
216 from noise outside of the room. The researcher remained in the room during the trial, but a wall
217 was placed between the arena and the experimenter to prohibit mice from seeing the researcher.
218 Mice were handled for 3 days for 1-2 minutes per day before experimentation began to reduce
219 handling anxiety. All behavioral analyses were recorded and analyzed using Noldus Ethovision
220 XT software.
221
222 **Locomotion**
223 Mice were placed in a 43cm x 43cm open field and allowed to explore for 30 minutes. The
224 center point of the mouse was tracked, and the primarily dependent variable was total locomotion
225 during the trial. Other tracked variables were average and maximum velocity, center entrances,
226 time spent in center, and locomotion binned into 1-minute periods to examine evolution of
227 exploration of the space.

228 **Novel Object Recognition**

229 Mice were placed in a 43cm x 43cm chamber with two similar objects and allowed 20
230 seconds of total familiarization time (nose point within 2cm radius of object), or 5 total minutes in
231 the chamber, whichever came first, before being returned to home cage. After 24 hours, mice
232 were allowed to explore the test space containing one object from the familiarization trial (familiar
233 object) and one novel object until total object interaction time of 20 seconds was reached. If 20
234 seconds of total interaction time was not reached before the 5-minute time limit, the trial was
235 excluded (3 trials). Mice that were climbing on objects were gently but quickly moved back to the
236 starting position.

237

238 **Novelty T-Maze**

239 The protocol was adapted from (Sanderson et al., 2009). Mice were placed in the "start"
240 arm of a T-shaped maze. The dimensions of each transparent arm were 30cm×10cm×20cm
241 (L×W×H). During training, the entrance to one arm ("novel arm", assignment counterbalanced
242 across groups) was blocked with clear plastic. Training consisted of five, 2-minute trials in which
243 each subject was allowed to explore the "start" and "familiar" arms. The training trials were
244 separated by a 1-minute inter-trial interval. After the training sessions, the plastic blocking the
245 "novel" arm was removed and mice were allowed to explore all arms of the maze. The test
246 session began when the center point of the mouse left the start arm and ended when 2 minutes
247 of total time was spent in the novel or familiar arm. Mice that showed anxiety-related behavior
248 and an aversion to either arm during the test (no arm entrances, <250cm total movement) were
249 excluded (2 mice).

250

251 **3-Chamber Social Interaction**

252 Mice were placed in the center chamber of a transparent 3-chamber arena and allowed 3
253 minutes to habituate to the space. The mouse was then placed into the closed center chamber

254 and the trial was started by removing the doors and allowing 15 minutes to explore the “social” or
255 “empty” chamber (Part I). The social chamber had a sex-matched, naïve mouse (4-5 weeks of
256 age) in a cylindrical interaction cage, while the empty chamber had only the interaction cage. The
257 chamber time and interaction time was recorded, with interaction time being defined as
258 experimental mouse nose point being within interaction zone (5cm from interaction cage).
259 Immediately after Part I, a novel mouse, also sex-matched and naïve, was introduced in the empty
260 cage and mice were allowed 15 minutes to explore “Novel” or “Familiar” chamber (Part II). The
261 familiar mouse is the social mouse from Part I. The locations of the novel and familiar mice were
262 switched to reduce side preference for this interaction partner.
263
264 **Barnes Maze**
265 The protocol was adapted from (Pitts, 2018). The Barnes maze apparatus is a 122cm-
266 diameter, white-acrylic circle with 40 evenly spaced, 5cm holes drilled 2.5cm from the edge of the
267 circle. This experiment was done in light room conditions to increase the motivation to escape.
268 The volume of the white noise was also increased (90dB). Four visual cues were placed on each
269 side of the platform, which consisted of brightly colored shapes (purple diamond, yellow star,
270 green cube, red triangle).
271 The mouse was first habituated to the escape tunnel, a small box filled with Alphadry
272 bedding, in its home cage for 1 minute. It was then habituated to the experimental conditions. The
273 mouse was placed in the center of the apparatus and allowed to explore until it entered the escape
274 tunnel or 5 minutes elapsed. If the mouse did not organically reach the escape tunnel within the
275 time limit, it was led to the exit. There was at least 1 hour between habituation and the onset of
276 acquisition training. The escape tunnel was moved between habituation and training trials.
277 There were 4 training trials per day for 4 consecutive days. There was an inter-trial interval
278 of 30 minutes. During training trials, the position of the escape tunnel remained at a fixed location
279 relative to the spatial cues. The mouse was placed in the center of the platform and tracked until

it fully entered the escape tunnel or 5 minutes elapsed. If the mouse failed to reach the escape tunnel in the allotted time, it was led to the escape by the researcher. Following each trial, the platform was cleaned with 70% alcohol and the bedding inside the escape chamber was replaced.

For each trial, several variables were tracked to assess performance. These include distance traveled, latency to exit, incorrect hole visits (primary errors), and incorrect hole revisits (secondary errors). Errors are defined as nose point entering a hole that does not contain the exit. Finally, based on these errors, the search strategy was characterized. Mice searched the maze serially, spatially, or randomly. Serial searching mice spent most of the time on the periphery performing a systematic search of the holes in a clockwise or counterclockwise manner, with 2 or less direction changes. Spatial search strategy was defined as <10 primary errors and a significantly reduced path and latency to exit. These mice use the surroundings to determine the shortest path to the exit and often are within 1-2 holes of the destination. All other results were defined as random search strategy. Random search strategy was usually characterized by multiple direction changes and skipping between holes, with many primary and secondary errors.

24 hours after the last training trial, mice were tested with a probe trial. The escape tunnel was removed before the mouse was placed on the platform for 5 minutes. Total time spent in each quartile was recorded, along with visits to former correct and incorrect escapes.

Light/Dark Box

Mice were placed in the light side of a Light/Dark box apparatus and movement within the apparatus was recorded from above for 10 minutes. The “light” side of the box had translucent walls and no ceiling, illuminated by the overhead room light. The “dark” side had opaque walls and a visible-light-filtering ceiling, allowing the mouse to experience a dark environment but the infrared camera to continue recording. We recorded the latency to enter the dark, transitions between zones, and time spent in zones.

306 **Elevated Plus Maze**

307 The elevated plus maze apparatus is a white “+”-shaped platform elevated 50cm above
308 the floor with oppositely positioned “open” arms and “closed” arms. The closed arms are enclosed
309 by 30cm high opaque walls, while the open arms have no railing. Each mouse was tested for 5
310 min after being placed onto the center platform facing an open arm. The number of open and
311 closed arm entries and the time spent on the various sections of the EPM was recorded. The
312 amount of exploration into the open arm is calculated to measure anxiety-like behavior.

313

314 **Stereotaxic Surgery**

315 Mice underwent stereotaxic surgery as described in (Ehinger et al., 2021). Specifically,
316 mice were anesthetized by vaporized isoflurane and were then headfixed in a stereotaxic frame
317 (David Kopf Instruments). The experimental virus, or relevant control, was infused into the dorsal
318 hippocampus (anteroposterior (AP) -2.3, mediolateral (ML) ±1.7, dorsoventral (DV) -1.7 mm
319 measured from bregma) using stainless steel injectors (33 gauge; Small Parts Incorporated)
320 connected to Hamilton syringes (10 µl, 1701). Animals received 1µl of virus bilaterally at a rate of
321 0.1µl/min controlled by an automatic pump (Harvard Apparatus). After the infusion was complete,
322 the injectors remained at the site for 10 minutes to allow diffusion of the virus. Mice were allowed
323 to recover in their home cages for at least 3 weeks before testing to allow for maximal viral
324 expression.

325

326 **Confirmation of Viral Expression**

327 At the end of the experimental timeline, animals were euthanized via cervical dislocation
328 and the brains were removed. The brains were placed on ice and dissected into 1-mm coronal
329 sections. The fluorescent protein expressed by the virus (either GFP or mCherry) was visualized
330 using an EVOS FL tabletop fluorescent microscope (ThermoFisher Scientific). Images were taken

for future reference. Animals that failed to exhibit fluorescence associated with viral overexpression were excluded from the study (4 mice).

Statistical Analysis

Biochemical analysis Parametric tests were performed on data deemed by the D'Agostino-Pearson omnibus (K2) test to be derived from a normally distributed population. Data were analyzed using a two-tailed t-test with Welch's correction for normal populations. Mann-Whitney tests were performed on data derived from non-normal populations. The results were determined to be statistically significant if the p-value was less than 0.05.

Electrophysiology analysis Parametric tests were performed on data deemed to be derived from a normally distributed population. Unpaired t-tests were performed on the average measurement over the experimental period. When multiple intensities were used, a two-way repeated measures ANOVA was performed. *Post hoc* pairwise comparisons (Tukey's) were performed after a significant result in the ANOVA. The results were determined to be statistically significant if the p-value was less than 0.05.

Behavioral analysis Parametric tests were performed on data deemed to be derived from a normally distributed population. Behavioral experiments were first assessed using a three-way ANOVA with primary variables being genotype, sex, and experimental variable where appropriate. Where there was no significant difference between sexes, the data was consolidated by genotype. A two-way ANOVA was then performed on the consolidated data (genotype x experimental variable). *Post hoc* Šidák's multiple comparison's test was performed to measure experimental differences directly. When there was only one experimental variable, an unpaired t-test was performed. If the variance was unequal, Welch's correction was applied. The results were determined to be statistically significant if the p-value was less than 0.05.

355 **Results**

356 **Generation and characterization of Prosapip1(flx/flx) mice**

357 To elucidate the role of Prosapip1 in the CNS, we generated a mouse line with flox sites
358 flanking the Prosapip1 gene. Guide RNA binding sites were identified in intron 2 and in the 3' UTR
359 of exon 5 of Prosapip1 (*Lzts3*) (**Figure 1A**). PAGE purified Ultramer single stranded DNA oligos
360 that were homologous to the target loci in intron 2 and exon 5 (**Figure 1B**) were used as repair
361 templates.

362 To construct a conditional knockout of Prosapip1 in neurons, we crossed the homozygous
363 Prosapip1 floxed (Prosapip1(flx/flx)) mouse with a mouse line expressing Cre recombinase under
364 the control of a synapsin promoter (Syn1-Cre(+)). Male Prosapip1(flx/flx);Syn1-Cre(-/-) mice were
365 mated with female Prosapip1(flx/flx);Syn1-Cre(+/-) mice (**Figure 1C**), which generated
366 Prosapip1(flx/flx);Syn1-Cre(+) and Prosapip1(flx/flx);Syn1-Cre(-) mice, which were used as
367 controls. The neuronal knockout was confirmed using western blot analysis. As shown in **Figure**
368 **1D**, Prosapip1(flx/flx);Syn1-Cre(-) mice have Prosapip1 protein levels comparable to a C57BL/6
369 mouse, while Prosapip1(flx/flx);Syn1-Cre(+) show a complete knockout of Prosapip1 protein in
370 the dHP.

371 We examined the breeding history of the newly developed line to identify any
372 abnormalities. The litter sizes of Prosapip1(flx/flx);Syn1-Cre matings followed a normal
373 distribution with an average litter size between 5 and 6 (**Figure 1E, Table 1**). The proportion of
374 male and female pups were near expectations, with 52% of pups being male and 48% female
375 (**Figure 1F**). Inheritance of Syn1-Cre(+) was also split evenly, with 53% of pups from the line
376 being born with the transgene (**Figure 1G**). Body weight of male and female mice was monitored
377 every 2 weeks from birth to assess potential developmental effects. While males were significantly
378 heavier than females throughout development, there was no significant effect of the genotype on
379 weight over time (**Figure 1H, Table 1**).

380 We next assessed baseline locomotor and exploratory behavior of these mice. Upon
381 reaching adulthood, mice were placed in an open field and allowed to explore for 20 minutes, and
382 total distance traveled and time spent in the center of the open field were measured. Deletion of
383 neuronal Prosapip1 did not alter locomotor activity (**Figure 1I, Table 1**). Furthermore, there were
384 no differences between genotypes when assessing the time spent in the center of the open field
385 (**Figure 1J, Table 1**).
386
387 **Prosapip1 is required for synaptic localization of PSD proteins**
388 Prosapip1 is a scaffolding protein that recruits SPAR to the PSD and interconnects it with
389 Shank3 in primary hippocampal neurons (Wendholt et al., 2006; Reim et al., 2016). First, we
390 examined if the synaptic localization of SPAR was affected by Prosapip1 neuronal knockout. To
391 do this, we isolated the synaptic fraction from the total homogenate. We confirmed the efficacy of
392 the crude synaptosomal fraction isolation by measuring enrichment of synapsin, a protein found
393 at the synapse, and lack of cAMP response element-binding protein (CREB), a transcription factor
394 located in the nucleus (**Figure 2A**). We analyzed the total (**Figure 2B**) and synaptic (**Figure 2C**)
395 levels of SPAR in the dHP of Prosapip1(flx/flx);Syn1-Cre(-) and Prosapip1(flx/flx);Syn1-Cre(+)
396 male and female mice. Total levels of SPAR were similar between the groups (**Figure 2B, Table**
397 **1**). However, we detected a significant reduction in synaptic SPAR in Prosapip1(flx/flx);Syn1-
398 Cre(+) mice as compared to the Prosapip1(flx/flx);Syn1-Cre(-) group (**Figure 2C, Table 1**).
399 Prosapip1 interconnects SPAR to Shank3, and SPAR forms a complex with PSD-95
400 (Wendholt et al., 2006; Reim et al., 2016; Matsuura et al., 2022). Therefore, we next examined
401 the total and synaptic levels of Shank3 and PSD-95. Prosapip1 deletion did not affect the total or
402 synaptic levels of Shank3 (**Figure 2D-G, Table 1**). We also found that Prosapip1(flx/flx);Syn1-
403 Cre(+) mice have similar levels of total PSD-95 (**Figure 2D, 2H, Table 1**) compared to
404 Prosapip1(flx/flx);Syn1-Cre(-) controls. However, when examining synaptic PSD-95,
405 Prosapip1(flx/flx);Syn1-Cre(+) mice displayed drastically reduced levels compared to controls

406 (**Figure 2E, 2I, Table 1**). Collectively, these results imply that Prosapip1 in the dHP is necessary
407 for synaptic localization of SPAR and PSD-95, but not Shank3.

408 SPAR and Shank3 are both known to interact with the NMDAR and AMPAR, and PSD-95
409 stabilizes NMDAR surface localization (Naisbitt et al., 1999; Tu et al., 1999; Pak et al., 2001;
410 Boeckers et al., 2002; Arons et al., 2012; Won et al., 2016; Coley and Gao, 2019; Matsuura et al.,
411 2022). As the synaptic localization of SPAR and PSD-95 is disrupted in the absence of Prosapip1,
412 we next tested the synaptic levels of NMDAR subunits GluN2A and GluN2B, along with AMPAR
413 subunit GluA1. There was no change in the overall levels of the NMDAR subunits GluN2A and
414 GluN2B or the AMPAR subunit GluA1 (**Figure 2J, 2L, 2N, 2P, Table 1**). The synaptic levels of
415 GluN2A and GluA1 were also unaltered in the dHP of Prosapip1(flx/flx);Syn1-Cre(+) mice
416 compared to Prosapip1(flx/flx);Syn1-Cre(-) controls (**Figure 2K, 2M, 2Q, Table 1**). In contrast, the
417 synaptic levels of NMDAR subunit GluN2B were significantly reduced in Prosapip1(flx/flx);Syn1-
418 Cre(+) mice (**Figure 2K, 2Q, Table 1**). Together, Prosapip1 controls the synaptic localization of
419 NMDAR subunit GluN2B, but not GluN2A or GluA1, in the dHP.

420

421 **Prosapip1 in the dorsal hippocampus plays a role in NMDA receptor-mediated**
422 **transmission and long-term potentiation**

423 The GluN2B subunit of the NMDAR is critically involved in learning and memory, a
424 process reliant on LTP (Nachtigall et al., 2024) Therefore, we examined the contribution of
425 Prosapip1 to GluN2B-mediated LTP. To examine this, hippocampal slices from male and female
426 Prosapip1(flx/flx);Syn1-Cre(-) and Prosapip1(flx/flx);Syn1-Cre(+) mice were prepared for
427 electrophysiology recordings. Bipolar stimulating electrodes were positioned in the CA1 region of
428 the dHP. Simultaneously, the recording electrode was placed approximately 100-150 μm away
429 from the stimulating electrode (**Figure 3A**). The administration of a single electrical pulse (2 ms)
430 elicited a fiber volley, followed by a field excitatory postsynaptic potential response (fEPSPs)
431 (**Figure 3B**). Before inducing LTP, a stable baseline of fEPSPs was established for 10 minutes

432 (**Figure 3C**). Upon establishing a baseline of fEPSPs, high-frequency stimulation (HFS) was
433 applied at 100 Hz for 1 second, repeated four times at 20-second intervals, to trigger LTP. In the
434 control Prosapip1(flx/flx);Syn1-Cre(-) mice, there was a significant increase in the fEPSP
435 amplitude following HFS, indicating a successful LTP induction (**Figure 3C**), which persisted for
436 at least 30 minutes (**Figure 3C**). However, LTP was absent in the Prosapip1(flx/flx);Syn1-Cre(+)
437 mice (**Figure 3C**). A comparative analysis of the normalized fEPSPs, conducted 20-30 minutes
438 post-HFS, revealed a significantly reduced fEPSP amplitude in the Prosapip1(flx/flx);Syn1-Cre(+)
439 group compared to the Prosapip1(flx/flx);Syn1-Cre(-) controls (**Figure 3D, Table 1**). Together
440 these findings strongly suggest Prosapip1 plays an important role in dHP LTP.

441 LTP induction in the hippocampus is known to rely on the functioning of postsynaptic
442 NMDARs. Therefore, we aimed to discern if there were any differences between
443 Prosapip1(flx/flx);Syn1-Cre(-) and Prosapip1(flx/flx);Syn1-Cre(+) mice in terms of NMDAR-
444 mediated excitatory postsynaptic currents (EPSCs) in dHP CA1 pyramidal neurons. A whole-cell
445 voltage-clamp recording technique was employed for this purpose. First, a low concentration of
446 external Mg^{2+} (0.05 mM) was used to facilitate the removal of the magnesium block from the
447 NMDAR channel. Concurrently, AMPARs and $GABA_A$ receptors ($GABA_A$Rs) were
448 pharmacologically inhibited. NMDAR-EPSCs were recorded in response to an escalating series
449 of stimulus intensities. The amplitude of NMDAR-EPSCs was significantly reduced in the
450 Prosapip1(flx/flx);Syn1-Cre(+) mice compared to the controls (**Figure 3E, Table 1**). Next, we
451 investigated whether LTP inhibition because of Prosapip1 deletion is due to post and/or
452 presynaptic changes. First, we investigated postsynaptic changes by measuring NMDA-induced
453 currents. NMDA (20 μM) was bath applied for 30 seconds and peak current was measured. We
454 observed that the peak current in the Prosapip1(flx/flx);Syn1-Cre(+) mice was markedly lower
455 than that in their control counterparts (**Figure 3F, Table 1**). These data suggest that postsynaptic
456 NMDAR responsiveness was decreased the in the dHP of Prosapip1(flx/flx);Syn1-Cre(+) mice as
457 compared to Prosapip1(flx/flx);Syn1-Cre(-) mice. Finally, to examine the presence of any

458 presynaptic alterations in glutamatergic transmission in CA1 neurons upon Prosapip1 deletion,
459 we measured the paired-pulse ratio (PPR, 100 millisecond interval) of electrically evoked EPSCs
460 in CA1 dHP neurons. Surprisingly we found that PPR was significantly higher in the
461 Prosapip1(flx/flx);Syn1-Cre(+) group as compared to Prosapip1(flx/flx);Syn1-Cre(-) mice (**Figure**
462 **3G, Table 1**), indicating a probable reduction in presynaptic glutamate release onto CA1 neurons
463 in the Prosapip1(flx/flx);Syn1-Cre(+) mice (Zucker and Regehr, 2002). Together, the data imply
464 that the Prosapip1 is crucial for the induction of hippocampal LTP, which is likely attributed to the
465 downregulation of NMDAR function.
466
467 **Prosapip1 contributes to spatial memory**
468 Prosapip1 was originally identified in hippocampal neurons (Wendholt et al., 2006; Reim
469 et al., 2016), a brain region associated with memory (Broadbent et al., 2004). Given the altered
470 PSD composition and subsequent loss of LTP in this region after Prosapip1 knockout, we
471 hypothesized that Prosapip1 contributes to memory-dependent behavior. First, we tested whether
472 Prosapip1 contributes to long-term recognition memory in male and female mice using the novel
473 object recognition (NOR) test with an inter-trial interval of 24 hours (Leger et al., 2013; Lueptow,
474 2017). Prosapip1(flx/flx);Syn1-Cre(-) animals showed a significant preference for the novel object,
475 indicating long-term memory of the familiar object and its spatial location (**Figure 4A, Table 1**).
476 Contrarily, male and female Prosapip1(flx/flx);Syn1-Cre(+) mice spent a similar amount of time
477 exploring both objects, performing at chance levels (**Figure 4A, Table 1**). The lack of novel object
478 recognition in Prosapip1 knockout mice implies a loss of object characteristic acquisition or long-
479 term recognition memory.

480 To determine whether Prosapip1 contributes to spatial learning or working memory, male
481 and female mice performed a novelty T-maze test (d'Isa et al., 2021). Mice were allowed to
482 explore two arms of a “T”-shaped maze during training trials while the third arm was blocked. All

483 three arms were available during the test. The experiment utilized a 1-minute inter-trial interval,
484 performance of which is reliant on hippocampal LTP (Sanderson et al., 2009). During the test trial,
485 Prosapip1(flx/flx);Syn1-Cre(-) mice primarily explored the novel arm of the T-maze, indicated by
486 a positive difference score (time spent in novel arm – time spent in familiar arm) (**Figure 4B,**
487 **Table 1**). Prosapip1(flx/flx);Syn1-Cre(+) mice explored the arms at comparable levels, performing
488 significantly worse than control animals, and indicating a lack of spatial learning for the familiar
489 arm of the maze (**Figure 4B, Table 1**). This difference can be seen visually in the heatmap
490 (**Figure 4C**). Taken together, these data suggest that Prosapip1 is required for spatial learning
491 and working memory.

492 We next utilized the 3-chamber social interaction (3CSI) test. The 3CSI test has two
493 stages. The first part measures the preference for social interaction with a juvenile interaction
494 partner. We found that male and female Prosapip1(flx/flx);Syn1-Cre(-) and
495 Prosapip1(flx/flx);Syn1-Cre(+) mice behave similarly, with both significantly preferring the
496 interaction partner over the empty chamber (**Figure 4D, Table 1**). In the second stage of the
497 3CSI, the mouse has the choice between interacting with a familiar partner (partner from part 1)
498 or a novel interaction partner. This assesses the social novelty recognition of the subject.
499 Prosapip1(flx/flx);Syn1-Cre(-) mice displayed a preference for the novel interaction partner,
500 exhibited by the increase in time spent in close proximity to the novel partner (**Figure 4E, Table**
501 **1**). Prosapip1(flx/flx);Syn1-Cre(+) mice spent a similar amount of time with the familiar and novel
502 interaction partners (**Figure 4E, Table 1**). The lack of discrimination from Prosapip1(flx/flx);Syn1-
503 Cre(+) mice implies a loss of recognition of social novelty or loss of social memory.

504 While the Prosapip1(flx/flx);Syn1-Cre(+) mice show impaired performance in the NOR and
505 novelty T-maze tests, these results may be attributed to the learning/acquisition process or
506 storage of memory. To confirm that Prosapip1 is important for processes underlying spatial
507 learning and memory, we employed the Barnes maze (Pitts, 2018). The Barnes maze is a white

508 plastic circle with holes evenly drilled around the perimeter. Underneath one of these holes is an
509 exit tunnel. The protocol has a training and testing phase, where spatial learning and memory,
510 respectively, are separately examined. First, mice were habituated to the platform. There were no
511 differences in baseline exploratory profile between Prosapip1(flx/flx);Syn1-Cre(-) and
512 Prosapip1(flx/flx);Syn1-Cre(+) mice (**Extended Figure 4A, Table 1**). The primary variable
513 examined during training trials was the path to escape, which tracked the distance traveled from
514 the starting point to the exit compartment. A shorter path to escape is more efficient and indicates
515 learning of the paradigm objective and exit location. Prosapip1(flx/flx);Syn1-Cre(-) mice
516 immediately improve performance, with a significant decrease in path to escape observed as
517 soon as the third trial (**Figure 4F, Table 1**). Prosapip1(flx/flx);Syn1-Cre(+) mice improved
518 performance over time but more gradually and performed significantly worse than control mice
519 over the entirety of training (**Figure 4F, Table 1**). Prosapip1(flx/flx);Syn1-Cre(-) mice showed a
520 significantly reduced path to escape by the second trial (**Figure 4F, Table 1**). In addition,
521 Prosapip1(flx/flx);Syn1-Cre(+) mice committed significantly more primary (incorrect hole visit) and
522 secondary (incorrect hole revisit) errors throughout training (**Figure 4G, Table 1**).

523 Differences in training performance can be explained by examining the search strategy of
524 each mouse. There are three defined search strategies: random, serial, and spatial, which
525 correspond to an increase in task efficiency (**Figure 4H**) (Rosenfeld and Ferguson, 2014). Mice
526 searching serially methodically inspected holes with minimal directional changes (Rosenfeld and
527 Ferguson, 2014). Spatial searchers used environmental cues to navigate efficiently to the exit
528 with less than 10 primary errors (Rosenfeld and Ferguson, 2014). In contrast, random search
529 strategies involved frequent direction changes and errors, with mice often skipping between holes
530 (Rosenfeld and Ferguson, 2014). Prosapip1(flx/flx);Syn1-Cre(-) mice mainly searched randomly
531 during the first trial, but 66% of mice utilized a serial search strategy by the second trial (**Figure
532 4I**). Spatial searching appeared as early as trial 3, and its ratio increased until it had become a

533 majority on the last day of training, with 77% of mice spatially searching on the final trial (**Figure**
534 **4I**). In the Prosapip1(flx/flx);Syn1-Cre(+) mice, randomly searching was a prevalent strategy
535 throughout training, with 39% of all trials being classified as random (**Figure 4J, Table 1**). More
536 than 50% of Prosapip1(flx/flx);Syn1-Cre(+) mice switched to serial search strategy by the third
537 day of training, which also explains the gradual decrease in path to escape (**Figure 4J, Table 1**).
538 Interestingly, less than 2% of all trials completed by Prosapip1(flx/flx);Syn1-Cre(+) mice utilized
539 the spatial search strategy (**Figure 4J, Table 1**). Both groups remember the context of the Barnes
540 maze and the objective to escape, but Prosapip1(flx/flx);Syn1-Cre(+) mice fail to remember the
541 spatial location of the exit. These results confirm the conclusion that Prosapip1 is required for
542 spatial learning.

543 The probe trial of the Barnes maze specifically assesses the spatial memory of the mouse.
544 During the probe trial, the exit was removed, and the mouse was allowed to explore the platform
545 for 5 minutes. If the mouse retained spatial memory of the exit, it spent significantly more time
546 exploring the quartile associated with the exit compartment compared to chance (25% of the
547 time). Control mice performed above chance value, spending an average of 116.84 seconds in
548 the exit quartile (**Figure 4K, Table 1**). Prosapip1(flx/flx);Syn1-Cre(+) mice, conversely, performed
549 around chance, spending an average of 68.52 seconds in the exit quartile (**Figure 4K, Table 1**).
550 This was significantly less than control mice and can be observed in the probe trial heat map
551 (**Figure 4L**). Thus, Prosapip1 is required for spatial memory in the Barnes maze.

552 To exclude the possibility that Prosapip1(flx/flx);Syn1-Cre(+) mice preferred familiar
553 situations compared to novel situations due to an increase in anxiety, we used the light/dark box
554 and elevated plus maze paradigms to assess the baseline anxiety of these mice. The light/dark
555 box consists of two chambers where the subject may choose to explore the well-lit ("light") or
556 visible-light-blocked ("dark") side of a chamber (Bourin and Hascoet, 2003). Spending less time
557 in the light side of the chamber implies an increase in anxiety (Bourin and Hascoet, 2003). Both

558 Prosapip1(flx/flx); Syn1-Cre(-) and Prosapip1(flx/flx);Syn1-Cre(+) mice spent significantly more
559 time in the dark side compared to the light side, but there was no significant difference between
560 the genotypes (**Extended Figure 4B, Table 1**). Mice also underwent the elevated plus maze test.
561 The elevated plus maze is elevated above the floor and consists of two "closed" arms with opaque
562 walls and two "open" arms with no railing. Time exploring the open arm is used to assess anxiety
563 (Walf and Frye, 2007). Prosapip1(flx/flx);Syn1-Cre(-) and Prosapip1(flx/flx);Syn1-Cre(+) mice
564 spent a similar amount of time exploring the open arm (**Extended Figure 4C, Table 1**). Taken
565 together, our data suggest that Prosapip1 is not involved in anxiety-related behaviors.
566

567 **Prosapip1 in the dorsal hippocampus contributes to recognition, social, and spatial**
568 **memory**

569 Memory is often associated with the dHP (Pilly and Grossberg, 2012). As our data suggest
570 that Prosapip1 contributes to recognition, social, and spatial memory, we next determined
571 whether the dHP is the loci of Prosapip1's contribution to learning and memory processes. To do
572 so, the dHP of Prosapip1(flx/flx) mice was infected with an adeno-associated virus (AAV)
573 expressing Cre to knockout Prospaip1 specifically in this region. An AAV expressing solely GFP
574 was used as a control (**Figure 5A**). Western blot analysis of the AAV-Cre-infected dHP shows
575 efficient deletion of Prosapip1 protein (**Figure 5B**).

576 We repeated the experimental battery performed on the genetically manipulated mice on
577 the mice infused with AAV-GFP or AAV-Cre in the dHP. In the open field, AAV-GFP- and AAV-
578 Cre-infected mice exhibited similar levels of locomotion (**Figure 5C, Table 1**) and spent a similar
579 amount of time in the center of the field (**Figure 5D, Table 1**). The region-specific knockout of
580 Prosapip1 did not affect exploratory behavior. We also directly assessed anxiety-like behavior
581 using the light/dark box. Mice infected with AAV-GFP or AAV-Cre both spent comparable amounts
582 of time in the light and dark chamber, preferring the dark (**Figure 5E, Table 1**). Therefore,
583 Prosapip1 in the dHP does not control locomotion or anxiety-like behavior.

584 Next, we examined the role of Prosapip1 in the dHP on memory. We first assessed
585 recognition memory using the novel object recognition test. The AAV-GFP-infected mice showed
586 a significant preference for the novel object, indicating functioning long-term recognition memory
587 (**Figure 5F, Table 1**). Mice infected with AAV-Cre, however, showed no significant preference for
588 either object (**Figure 5F, Table 1**). Similarly, in the novelty T-maze test, AAV-GFP-infected mice
589 spent much of the test exploring the novel arm of the maze, indicated by a positive difference
590 score (**Figure 5G, Table 1**). AAV-Cre-infected mice spent significantly less time exploring the
591 novel arm of the maze, performing at chance levels (**Figure 5G, Table 1**). Together, these results
592 suggest that Prosapip1 in the dHP specifically contributes to recognition and spatial working
593 memory.
594 We also assessed the effects of region-specific Prosapip1 knockout on sociability and
595 social memory using the 3-chamber social interaction test. Both AAV-GFP- and AAV-Cre-infected
596 mice showed a significant preference for interacting with a social partner over the empty cage
597 (**Figure 5H, Table 1**). When a novel interaction partner was introduced, AAV-GFP mice
598 significantly preferred interacting with the novel partner (**Figure 5I, Table 1**). AAV-Cre-infected
599 mice did not show a significant preference (**Figure 5I, Table 1**).
600 Finally, AAV-GFP- and AAV-Cre-infected mice underwent the Barnes maze procedure to
601 separately assess spatial learning and memory. During training trials, AAV-Cre-infected mice
602 performed significantly worse when examining path to escape (**Figure 5J, Table 1**). While AAV-
603 GFP-infected mice quickly improved exit strategy, AAV-Cre-infected mice were more variable and
604 took a longer path, on average (**Figure 5J, Table 1**). After training, during the probe trial, that
605 AAV-GFP-infected mice spent significantly more time in the exit quartile compared to AAV-Cre-
606 infected mice (**Figure 5K, Table 1**). Together, our data suggests that Prosapip1 in the dHP is
607 specifically involved in the formation of spatial memory.
608

609 **Discussion**

610 Our findings suggest that Prosapip1 in the dHP is responsible for the synaptic localization
611 of SPAR and PSD-95, and consequently, for the membranal localization of GluN2B. Furthermore,
612 our data suggest that Prosapip1 in the dHP plays an important role in LTP as well as learning and
613 memory.

614

615 **Prosapip1 is a key protein in the PSD**

616 Prosapip1 is highly enriched in the PSD of primary hippocampal neurons (Wendholt et al.,
617 2006; Reim et al., 2016), and our results suggest that Prosapip1 could be crucial to the formation
618 and stability of PSD complexes. Prosapip1 scaffolds SPAR to Shank3 in the PSD (Wendholt et
619 al., 2006; Dolnik et al., 2016; Reim et al., 2016). We found that knockout of Prosapip1 reduced
620 the synaptic localization of SPAR but not Shank3. Reim et al. reported that Prosapip1 is directly
621 regulating SPAR levels in the PSD in primary hippocampal neurons (Reim et al., 2016). Our data
622 supports this study, as Prosapip1 knockout *in vivo* led to a reduction of synaptic SPAR. SPAR
623 plays a role in the formation of F-actin, which is important for dendritic spine maturation (Pak et
624 al., 2001). We previously showed Prosapip1 interacts with SPAR in the NAc of mice (Laguesse
625 et al., 2017), and Prosapip1 knockdown reduces F-actin content while overexpression increases
626 F-actin content in the NAc (Laguesse et al., 2017). Furthermore, we showed that Prosapip1 plays
627 a role in spine maturation in the NAc (Laguesse et al., 2017). Our results suggest that the
628 recruitment of SPAR to the PSD via Prosapip1 in the dHP will promote F-actin formation and lead
629 to dendritic spine maturation, however these possibilities merit further examined.

630 Both SPAR and Shank3 interact with PSD-95 (Naisbitt et al., 1999; Tu et al., 1999; Pak et
631 al., 2001). SPAR binds PSD-95 directly (Pak et al., 2001), and Shank3 associates with Guanylate
632 kinase-associated protein (GKAP), which binds PSD-95 (Naisbitt et al., 1999; Tu et al., 1999).

633 PSD-95 binds to NMDAR subunits GluN2A and GluN2B and stabilizes NMDAR surface
634 localization (Won et al., 2016; Coley and Gao, 2019). Studies have shown that PSD-95 deficiency
635 causes an imbalance of NMDAR and AMPAR synaptic presence, altering glutamatergic
636 transmission (Lin et al., 2004; Elias et al., 2006; Zhang et al., 2013; Chen et al., 2015).
637 Surprisingly, we discovered that loss of Prosapip1 resulted in a marked reduction of synaptic
638 PSD-95, and a correlated reduction in the synaptic compartmentalization of the NMDAR subunit
639 GluN2B, raising the possibility that the interaction between Prosapip1 and PSD-95 is required for
640 synaptic membranal localization of GluN2B. However, we did not observe a change in the
641 synaptic level of GluN2A. In addition, we did not find that the localization of the AMPAR subunit
642 GluA1 was altered as a result of Prosapip1 knockout. In line with our findings, Pak et al. showed
643 that SPAR binds PSD-95 and GluN2B, but not GluA1 (Pak et al., 2001). Based on our results and
644 these studies, the complex controlling AMPAR synaptic localization is different, and likely
645 independent of Prosapip1 in the dHP. Together, our data suggest that Prosapip1 is necessary for
646 the formation and/or maintenance of the NMDAR-associated PSD network.

647 We previously discovered that Prosapip1's translation depends on mTORC1 in the NAc
648 of mice consuming excessive levels of alcohol, which in turn promotes F-actin formation, dendritic
649 spine maturation and alcohol-reward memory and the reinforcement of alcohol consumption
650 (Laguesse et al., 2017). mTORC1 activation by alcohol also induces the translation of the
651 scaffolding protein Homer and PSD-95 in the NAc of mice (Beckley et al., 2016; Liu et al., 2017).
652 mTORC1 plays an essential role in the translation of a subset of mRNAs to proteins. In the CNS,
653 mTORC1 promotes the translation of synaptic proteins at dendrites (Buffington et al., 2014), and
654 plays an important LTP, learning, and memory (Hoeffer and Klann, 2010; Graber et al., 2013).
655 Therefore, it would be of great interest to test the hypothesis that learning-dependent activation
656 of mTORC1 in the dHP activates the translational machinery at synapses and therefore increases

657 the translation of Prosapip1 which in turn recruits proteins such as PSD-95 to stabilize the PSD-
658 95 complex.

659

660 **Prosapip1 is required for LTP in the dHP**

661 In our study, we discovered that mice lacking Prosapip1 exhibited markedly diminished
662 NMDAR-mediated synaptic transmission, which is in line with the fact that there is reduced
663 synaptic GluN2B. We also found that Prosapip1 knockout led to a significant reduction in the
664 formation of LTP. LTP is a persistent increase in synaptic strength between neurons that can last
665 for months *in vivo* (Abraham et al., 2002; Cooke and Bliss, 2006) and is the cellular hallmark of
666 learning and memory. It is often induced by HFS, which causes extensive glutamate release and
667 significant AMPAR activity, resulting in large membrane depolarization (Ma et al., 2018). This
668 depolarization facilitates the removal of Mg^{2+} blockage in NMDARs, thereby activating them and
669 leading to calcium influx (Ma et al., 2018). This influx triggers the calmodulin/CaMKII pathway,
670 initiating a series of cascades that enhance AMPAR phosphorylation and trafficking, culminating
671 in sustained synaptic strengthening (Huganir and Nicoll, 2013; Herring and Nicoll, 2016).
672 Therefore, the induction of hippocampal LTP heavily relies on NMDAR activation, with alterations
673 in NMDAR function significantly affecting the establishment of hippocampal LTP and its
674 associated learning and memory processes. In Prosapip1 knockout mice, the reduction in
675 NMDAR functionality likely results in decreased calcium influx during high-frequency stimulation
676 and diminished activation of the calmodulin/CaMKII pathway, leading to weaker synaptic
677 strengthening.

678

679

680

681 **Prosapip1 is required for learning and memory**

682 As detailed above, we found that Prosapip1 neuronal knockout mice have deficits in LTP
683 in the dHP, and LTP is the hallmark of learning and memory (Bliss and Collingridge, 1993; Frey
684 and Morris, 1998; Collingridge et al., 2004). We also found that global neuronal knockout and
685 dHP-specific knockout of Prosapip1 results in deficits in spatial learning and memory. Specifically,
686 we showed that Prosapip1 in the dHP is required for normal performance in the novel object
687 recognition, novelty T-maze, 3-chamber social interaction, and Barnes maze tests, which all
688 require a unique form of learning and memory (Davis et al., 1992; Broadbent et al., 2010; Barker
689 and Warburton, 2011; Rosenfeld and Ferguson, 2014; Lueptow, 2017; Pitts, 2018; Sanchez-
690 Rodriguez et al., 2022). The novel object recognition test is primarily examining recognition
691 memory, and with an inter-trial interval of 24 hours, specifically long-term memory (Broadbent et
692 al., 2010; Barker and Warburton, 2011; Antunes and Biala, 2012; Lueptow, 2017; Cinalli et al.,
693 2020). The novelty T-maze focuses on both spatial learning and memory, and with its short, 1-
694 minute inter-trial interval, this procedure is examining spatial working memory (Sharma et al.,
695 2010; d'Isa et al., 2021). The 3-chamber social interaction test is assessing baseline sociability
696 and also social recognition memory (Meira et al., 2018; Tzakis and Holahan, 2019; Wang and
697 Zhan, 2022; Cope et al., 2023; Wei et al., 2024). Finally, the Barnes maze tests both spatial
698 learning and working memory in intra-day trials, while simultaneously testing long-term contextual
699 and spatial memory in inter-day trials and the probe test (Bach et al., 1995; Sharma et al., 2010;
700 Rosenfeld and Ferguson, 2014; Pitts, 2018). Interestingly, loss of hippocampal LTP has been
701 shown to impair spatial, but not contextual memory in the Barnes maze (Bach et al., 1995). As
702 presented here, Prosapip1 knockout mice significantly reduced distance traveled to exit but did
703 not switch to spatial searching. In this example, Prosapip1 knockout mice are retaining the
704 contextual understanding of escaping the platform, but do not recall the spatial location of the exit.
705 Additionally, the link between NMDAR function and learning and memory is well established

706 (Newcomer et al., 2000; Li and Tsien, 2009). For example, blockage of hippocampal NMDA
707 receptors impairs spatial learning in rats (Davis et al., 1992; Bye and McDonald, 2019). Prosapip1
708 is likely controlling the reinforcement of learning and memory by PSD scaffolding, stabilization,
709 and GluN2B synaptic localization, leading to LTP.

710 We observed that Prosapip1 knockout specifically in the dHP replicated the recognition,
711 social, and spatial learning and memory deficits exhibited by the global neuronal knockout mice,
712 suggesting that Prosapip1 is controlling these learning and memory processes specifically in the
713 dHP. The dHP primarily controls memory formation and recall (Eichenbaum, 1997; Broadbent et
714 al., 2004; Squire et al., 2004; Pilly and Grossberg, 2012). We found that LTP in the CA1 subregion
715 of the dHP was reliant on Prosapip1. The CA1 subregion is critically involved in contextual
716 memory, object recognition memory, and spatial memory (Tsien et al., 1996; Lee and Kesner,
717 2004; Daumas et al., 2005; Sanderson et al., 2009; Sharma et al., 2010; Stevenson et al., 2018;
718 Bye and McDonald, 2019; Cinalli et al., 2020; Jeong and Singer, 2022). Loss of Prosapip1 in CA1
719 is likely leading to decreased performance in the novel object recognition, novelty T-maze, and
720 Barnes maze tests. The lack of social recognition displayed by Prosapip1(flx/flx);Syn1-Cre(+)
721 mice and AAV-Cre-infected mice is likely attributed to the loss of Prosapip1 in the CA2 subregion
722 of the dHP, which is the primary subregion controlling social recognition memory (Meira et al.,
723 2018; Tzakis and Holahan, 2019; Wang and Zhan, 2022; Cope et al., 2023; Wei et al., 2024).
724 Specifically, silencing the CA2 subregion of the dHP impairs social memory formation and
725 consolidation (Meira et al., 2018). However, the CA3 and DG subregions of the dHP are also
726 involved in spatial and contextual memory (Broadbent et al., 2004; Lee and Kesner, 2004;
727 Daumas et al., 2005). As our conditional knockout strategy resulted in Prosapip1 deletion from
728 the whole dHP, further studies are required to dissect the subregion specificity of the contribution
729 of Prosapip1 to recognition, social, and spatial learning and memory processes.

730 Memory consists of three primary processes: encoding, consolidation, and retrieval
731 (Straube, 2012). In this study, the defect in memory function is likely due to a failure to encode
732 new information (Bye and McDonald, 2019) or consolidate this “short-term” into “long-term”
733 memory (Yang et al., 2022). The spatial T-maze experiment utilized a short inter-trial interval of
734 one minute which requires working spatial memory (Sharma et al., 2010), and Prosapip1 knockout
735 mice exhibited a failure to encode new information. Similarly, the Barnes maze training trials were
736 separated by an inter-trial interval of 30 minutes, but Prosapip1 knockout mice did not acquire
737 spatial memory between training trials, nor during the longer consolidation periods between days,
738 again implying a failure to encode spatial information or consolidate this information. The lack of
739 synaptic localization of GluN2B is likely underlying the loss of memory encoding or consolidation
740 (Nachtigall et al., 2024). It is unlikely that NMDAR dysfunction is affecting the retrieval of memory,
741 as studies have exhibited rats’ ability to use previously acquired spatial information during
742 NMDAR blockage (Bast et al., 2005; Mackes and Willner, 2006; Bye and McDonald, 2019).

743 Prosapip1 belongs to the Fezzin family of proteins (Wendholt et al., 2006). It is important
744 to note that other Fezzins do not compensate for the loss of Prosapip1 in the dHP. Knockout of
745 other Fezzins, like PSD-Zip70, also lead to cognitive deficits (Mayanagi et al., 2015). However,
746 these deficits were attributed to the action of PSD-Zip70 in the PFC. Therefore, one could
747 hypothesize that proteins in this family enact their function in specific brain subregions.

748 In summary, Prosapip1 in the dorsal hippocampus is integral to the synaptic localization
749 of SPAR, PSD-95, and GluN2B, which are required for the formation of LTP and subsequent
750 spatial learning and memory behavior. Abnormalities with PSD proteins are associated with
751 neuropsychiatric disorders (Kaizuka and Takumi, 2018), and further unraveling of the
752 physiological role of Prosapip1 may unlock insights into normal and abnormal mechanisms of
753 learning and memory.

754 **Funding and Disclosure:** Supported by NIH grant AA020889 (G.H.). ZWH was partially funded
755 by GM007175. None of the authors have a conflict of interest.

756

757 **Acknowledgements:** Some figures were created in part with BioRender.com. We thank Carolyn
758 Ferguson for expert technical assistance.

759

760 **Author Contributions:** DR conceived the project. GH developed the mouse line. ZWH, JW,
761 and DR designed the experiments. ZWH, HG, KP, and CS conducted the experiments and
762 analyzed the data. ZWH, HG, YE, JW, and DR wrote the manuscript.

763 **References**

764 Abraham WC, Logan B, Greenwood JM, Dragunow M (2002) Induction and experience-
765 dependent consolidation of stable long-term potentiation lasting months in the
766 hippocampus. J Neurosci 22:9626-9634.

767 Antunes M, Biala G (2012) The novel object recognition memory: neurobiology, test procedure,
768 and its modifications. Cogn Process 13:93-110.

769 Arons MH, Thynne CJ, Grabrucker AM, Li D, Schoen M, Cheyne JE, Boeckers TM, Montgomery
770 JM, Garner CC (2012) Autism-associated mutations in ProSAP2/Shank3 impair synaptic
771 transmission and neurexin-neuroligin-mediated transsynaptic signaling. J Neurosci
772 32:14966-14978.

773 Bach ME, Hawkins RD, Osman M, Kandel ER, Mayford M (1995) Impairment of spatial but not
774 contextual memory in CaMKII mutant mice with a selective loss of hippocampal LTP in the
775 range of the theta frequency. Cell 81:905-915.

776 Barker GR, Warburton EC (2011) When is the hippocampus involved in recognition memory? J
777 Neurosci 31:10721-10731.

778 Bast T, da Silva BM, Morris RG (2005) Distinct contributions of hippocampal NMDA and AMPA
779 receptors to encoding and retrieval of one-trial place memory. J Neurosci 25:5845-5856.

780 Beckley JT, Laguesse S, Phamluong K, Morisot N, Wegner SA, Ron D (2016) The First Alcohol
781 Drink Triggers mTORC1-Dependent Synaptic Plasticity in Nucleus Accumbens Dopamine
782 D1 Receptor Neurons. J Neurosci 36:701-713.

783 Bliss TV, Collingridge GL (1993) A synaptic model of memory: long-term potentiation in the
784 hippocampus. Nature 361:31-39.

785 Boeckers TM, Bockmann J, Kreutz MR, Gundelfinger ED (2002) ProSAP/Shank proteins - a
786 family of higher order organizing molecules of the postsynaptic density with an emerging
787 role in human neurological disease. J Neurochem 81:903-910.

788 Boeckers TM, Winter C, Smalla KH, Kreutz MR, Bockmann J, Seidenbecher C, Garner CC,
789 Gundelfinger ED (1999) Proline-rich synapse-associated proteins ProSAP1 and ProSAP2
790 interact with synaptic proteins of the SAPAP/GKAP family. Biochem Biophys Res
791 Commun 264:247-252.
792 Bourin M, Hascoet M (2003) The mouse light/dark box test. Eur J Pharmacol 463:55-65.
793 Broadbent NJ, Squire LR, Clark RE (2004) Spatial memory, recognition memory, and the
794 hippocampus. Proc Natl Acad Sci U S A 101:14515-14520.
795 Broadbent NJ, Gaskin S, Squire LR, Clark RE (2010) Object recognition memory and the rodent
796 hippocampus. Learn Mem 17:5-11.
797 Buffington SA, Huang W, Costa-Mattioli M (2014) Translational control in synaptic plasticity and
798 cognitive dysfunction. Annu Rev Neurosci 37:17-38.
799 Bye CM, McDonald RJ (2019) A Specific Role of Hippocampal NMDA Receptors and Arc Protein
800 in Rapid Encoding of Novel Environmental Representations and a More General Long-
801 Term Consolidation Function. Front Behav Neurosci 13:8.
802 Chen X, Levy JM, Hou A, Winters C, Azzam R, Sousa AA, Leapman RD, Nicoll RA, Reese TS
803 (2015) PSD-95 family MAGUKs are essential for anchoring AMPA and NMDA receptor
804 complexes at the postsynaptic density. Proc Natl Acad Sci U S A 112:E6983-6992.
805 Cinalli DA, Jr., Cohen SJ, Guthrie K, Stackman RW, Jr. (2020) Object Recognition Memory:
806 Distinct Yet Complementary Roles of the Mouse CA1 and Perirhinal Cortex. Front Mol
807 Neurosci 13:527543.
808 Coley AA, Gao WJ (2019) PSD-95 deficiency disrupts PFC-associated function and behavior
809 during neurodevelopment. Sci Rep 9:9486.
810 Collingridge GL, Isaac JT, Wang YT (2004) Receptor trafficking and synaptic plasticity. Nat Rev
811 Neurosci 5:952-962.
812 Concordet JP, Haeussler M (2018) CRISPOR: intuitive guide selection for CRISPR/Cas9 genome
813 editing experiments and screens. Nucleic Acids Res 46:W242-W245.

814 Cooke SF, Bliss TV (2006) Plasticity in the human central nervous system. Brain 129:1659-1673.
815 Cope EC, Wang SH, Waters RC, Gore IR, Vasquez B, Laham BJ, Gould E (2023) Activation of
816 the CA2-ventral CA1 pathway reverses social discrimination dysfunction in Shank3B
817 knockout mice. Nat Commun 14:1750.
818 d'Isa R, Comi G, Leocani L (2021) Apparatus design and behavioural testing protocol for the
819 evaluation of spatial working memory in mice through the spontaneous alternation T-
820 maze. Sci Rep 11:21177.
821 Daumas S, Halley H, Frances B, Lassalle JM (2005) Encoding, consolidation, and retrieval of
822 contextual memory: differential involvement of dorsal CA3 and CA1 hippocampal
823 subregions. Learn Mem 12:375-382.
824 Davis S, Butcher SP, Morris RG (1992) The NMDA receptor antagonist D-2-amino-5-
825 phosphonopentanoate (D-AP5) impairs spatial learning and LTP in vivo at intracerebral
826 concentrations comparable to those that block LTP in vitro. J Neurosci 12:21-34.
827 Dolnik A, Kanwal N, Mackert S, Halbedl S, Proepper C, Bockmann J, Schoen M, Boeckers TM,
828 Kuhl SJ, Schmeisser MJ (2016) Sipa1l3/SPAR3 is targeted to postsynaptic specializations
829 and interacts with the Fezzin ProSAPiP1/Lzts3. J Neurochem 136:28-35.
830 Ehinger Y, Morisot N, Phamluong K, Sakhai SA, Soneja D, Adrover MF, Alvarez VA, Ron D (2021)
831 cAMP-Fyn signaling in the dorsomedial striatum direct pathway drives excessive alcohol
832 use. Neuropsychopharmacology 46:334-342.
833 Eichenbaum H (1997) Declarative memory: insights from cognitive neurobiology. Annu Rev
834 Psychol 48:547-572.
835 Elias GM, Funke L, Stein V, Grant SG, Bredt DS, Nicoll RA (2006) Synapse-specific and
836 developmentally regulated targeting of AMPA receptors by a family of MAGUK scaffolding
837 proteins. Neuron 52:307-320.
838 Frey U, Morris RG (1998) Synaptic tagging: implications for late maintenance of hippocampal
839 long-term potentiation. Trends Neurosci 21:181-188.

840 Gangal H, Xie X, Huang Z, Cheng Y, Wang X, Lu J, Zhuang X, Essoh A, Huang Y, Chen R, Smith
841 LN, Smith RJ, Wang J (2023) Drug reinforcement impairs cognitive flexibility by inhibiting
842 striatal cholinergic neurons. Nat Commun 14:3886.
843 Graber TE, McCamphill PK, Sossin WS (2013) A recollection of mTOR signaling in learning and
844 memory. Learn Mem 20:518-530.
845 Herring BE, Nicoll RA (2016) Long-Term Potentiation: From CaMKII to AMPA Receptor
846 Trafficking. Annu Rev Physiol 78:351-365.
847 Hoeffer CA, Klann E (2010) mTOR signaling: at the crossroads of plasticity, memory and disease.
848 Trends Neurosci 33:67-75.
849 Horii T, Morita S, Kimura M, Terawaki N, Shibutani M, Hatada I (2017) Efficient generation of
850 conditional knockout mice via sequential introduction of lox sites. Sci Rep 7:7891.
851 Huganir RL, Nicoll RA (2013) AMPARs and synaptic plasticity: the last 25 years. Neuron 80:704-
852 717.
853 Jeong N, Singer AC (2022) Learning from inhibition: Functional roles of hippocampal CA1
854 inhibition in spatial learning and memory. Curr Opin Neurobiol 76:102604.
855 Kaizuka T, Takumi T (2018) Postsynaptic density proteins and their involvement in
856 neurodevelopmental disorders. J Biochem 163:447-455.
857 Kennedy MB (2018) The Protein Biochemistry of the Postsynaptic Density in Glutamatergic
858 Synapses Mediates Learning in Neural Networks. Biochemistry 57:4005-4009.
859 Kuriu T, Inoue A, Bito H, Sobue K, Okabe S (2006) Differential control of postsynaptic density
860 scaffolds via actin-dependent and -independent mechanisms. J Neurosci 26:7693-7706.
861 Labuhn M, Adams FF, Ng M, Knoess S, Schambach A, Charpentier EM, Schwarzer A, Mateo JL,
862 Klusmann JH, Heckl D (2018) Refined sgRNA efficacy prediction improves large- and
863 small-scale CRISPR-Cas9 applications. Nucleic Acids Res 46:1375-1385.
864 Laguesse S, Morisot N, Shin JH, Liu F, Adrover MF, Sakhai SA, Lopez MF, Phamluong K, Griffin
865 WC, 3rd, Becker HC, Bender KJ, Alvarez VA, Ron D (2017) Prosapip1-Dependent

866 Synaptic Adaptations in the Nucleus Accumbens Drive Alcohol Intake, Seeking, and
867 Reward. Neuron 96:145-159 e148.
868 Lee I, Kesner RP (2004) Differential contributions of dorsal hippocampal subregions to memory
869 acquisition and retrieval in contextual fear-conditioning. Hippocampus 14:301-310.
870 Leger M, Quiedeville A, Bouet V, Haelewyn B, Boulouard M, Schumann-Bard P, Freret T (2013)
871 Object recognition test in mice. Nat Protoc 8:2531-2537.
872 Li F, Tsien JZ (2009) Memory and the NMDA receptors. N Engl J Med 361:302-303.
873 Lin Y, Skeberdis VA, Francesconi A, Bennett MV, Zukin RS (2004) Postsynaptic density protein-
874 95 regulates NMDA channel gating and surface expression. J Neurosci 24:10138-10148.
875 Liu F, Laguesse S, Legastelois R, Morisot N, Ben Hamida S, Ron D (2017) mTORC1-dependent
876 translation of collapsin response mediator protein-2 drives neuroadaptations underlying
877 excessive alcohol-drinking behaviors. Mol Psychiatry 22:89-101.
878 Lueptow LM (2017) Novel Object Recognition Test for the Investigation of Learning and Memory
879 in Mice. J Vis Exp:55718.
880 Ma T, Cheng Y, Roltsch Hellard E, Wang X, Lu J, Gao X, Huang CCY, Wei XY, Ji JY, Wang J
881 (2018) Bidirectional and long-lasting control of alcohol-seeking behavior by corticostriatal
882 LTP and LTD. Nat Neurosci 21:373-383.
883 Mackes JL, Willner J (2006) NMDA antagonist MK-801 impairs acquisition of place strategies, but
884 not their use. Behav Brain Res 175:112-118.
885 Matsuura K, Kobayashi S, Konno K, Yamasaki M, Horiuchi T, Senda T, Hayashi T, Satoh K,
886 Arima-Yoshida F, Iwasaki K, Negishi L, Yasui-Shimizu N, Kohu K, Kawahara S, Kirino Y,
887 Nakamura T, Watanabe M, Yamamoto T, Manabe T, Akiyama T (2022) SIPA1L1/SPAR1
888 Interacts with the Neurabin Family of Proteins and is Involved in GPCR Signaling. J
889 Neurosci 42:2448-2473.

890 Mayanagi T, Yasuda H, Sobue K (2015) PSD-Zip70 Deficiency Causes Prefrontal Hypofunction
891 Associated with Glutamatergic Synapse Maturation Defects by Dysregulation of Rap2
892 Activity. J Neurosci 35:14327-14340.
893 Meira T, Leroy F, Buss EW, Oliva A, Park J, Siegelbaum SA (2018) A hippocampal circuit linking
894 dorsal CA2 to ventral CA1 critical for social memory dynamics. Nat Commun 9:4163.
895 Nachtigall EG, de CMJ, Izquierdo I, Furini CRG (2024) Cellular mechanisms of contextual fear
896 memory reconsolidation: Role of hippocampal SFKs, TrkB receptors and GluN2B-
897 containing NMDA receptors. Psychopharmacology (Berl) 241:61-73.
898 Naisbitt S, Kim E, Tu JC, Xiao B, Sala C, Valtschanoff J, Weinberg RJ, Worley PF, Sheng M
899 (1999) Shank, a novel family of postsynaptic density proteins that binds to the NMDA
900 receptor/PSD-95/GKAP complex and cortactin. Neuron 23:569-582.
901 Newcomer JW, Farber NB, Olney JW (2000) NMDA receptor function, memory, and brain aging.
902 Dialogues Clin Neurosci 2:219-232.
903 Pak DT, Yang S, Rudolph-Correia S, Kim E, Sheng M (2001) Regulation of dendritic spine
904 morphology by SPAR, a PSD-95-associated RapGAP. Neuron 31:289-303.
905 Pilly PK, Grossberg S (2012) How do spatial learning and memory occur in the brain? Coordinated
906 learning of entorhinal grid cells and hippocampal place cells. J Cogn Neurosci 24:1031-
907 1054.
908 Pitts MW (2018) Barnes Maze Procedure for Spatial Learning and Memory in Mice. Bio Protoc 8.
909 Qualmann B, Boeckers TM, Jeromin M, Gundelfinger ED, Kessels MM (2004) Linkage of the actin
910 cytoskeleton to the postsynaptic density via direct interactions of Abp1 with the
911 ProSAP/Shank family. J Neurosci 24:2481-2495.
912 Reim D, Weis TM, Halbedl S, Delling JP, Grabrucker AM, Boeckers TM, Schmeisser MJ (2016)
913 The Shank3 Interaction Partner ProSAPiP1 Regulates Postsynaptic SPAR Levels and the
914 Maturation of Dendritic Spines in Hippocampal Neurons. Front Synaptic Neurosci 8:13.

915 Renaud JB, Boix C, Charpentier M, De Cian A, Cochennec J, Duvernois-Berthet E, Perrouault L,
916 Tesson L, Edouard J, Thinard R, Cherifi Y, Menoret S, Fontaniere S, de Croze N,
917 Fraichard A, Sohm F, Anegon I, Concordet JP, Giovannangeli C (2016) Improved Genome
918 Editing Efficiency and Flexibility Using Modified Oligonucleotides with TALEN and
919 CRISPR-Cas9 Nucleases. Cell Rep 14:2263-2272.
920 Richter M, Murai KK, Bourgin C, Pak DT, Pasquale EB (2007) The EphA4 receptor regulates
921 neuronal morphology through SPAR-mediated inactivation of Rap GTPases. J Neurosci
922 27:14205-14215.
923 Rosenfeld CS, Ferguson SA (2014) Barnes maze testing strategies with small and large rodent
924 models. J Vis Exp:e51194.
925 Sanchez-Rodriguez I, Temprano-Carazo S, Jeremic D, Delgado-Garcia JM, Gruart A, Navarro-
926 Lopez JD, Jimenez-Diaz L (2022) Recognition Memory Induces Natural LTP-like
927 Hippocampal Synaptic Excitation and Inhibition. Int J Mol Sci 23:10806.
928 Sanderson DJ, Good MA, Skelton K, Sprengel R, Seeburg PH, Rawlins JN, Bannerman DM
929 (2009) Enhanced long-term and impaired short-term spatial memory in GluA1 AMPA
930 receptor subunit knockout mice: evidence for a dual-process memory model. Learn Mem
931 16:379-386.
932 Sharma S, Rakoczy S, Brown-Borg H (2010) Assessment of spatial memory in mice. Life Sci
933 87:521-536.
934 Sheng M, Kim E (2000) The Shank family of scaffold proteins. J Cell Sci 113 (Pt 11):1851-1856.
935 Squire LR, Stark CE, Clark RE (2004) The medial temporal lobe. Annu Rev Neurosci 27:279-306.
936 Stemmer M, Thumberger T, Del Sol Keyer M, Wittbrodt J, Mateo JL (2015) CCTop: An Intuitive,
937 Flexible and Reliable CRISPR/Cas9 Target Prediction Tool. PLoS One 10:e0124633.
938 Stevenson RF, Zheng J, Mnatsakanyan L, Vadera S, Knight RT, Lin JJ, Yassa MA (2018)
939 Hippocampal CA1 gamma power predicts the precision of spatial memory judgments.
940 Proc Natl Acad Sci U S A 115:10148-10153.

941 Straube B (2012) An overview of the neuro-cognitive processes involved in the encoding,
942 consolidation, and retrieval of true and false memories. Behav Brain Funct 8:35.
943 Tsien JZ, Huerta PT, Tonegawa S (1996) The essential role of hippocampal CA1 NMDA receptor-
944 dependent synaptic plasticity in spatial memory. Cell 87:1327-1338.
945 Tu JC, Xiao B, Naisbitt S, Yuan JP, Petralia RS, Brakeman P, Doan A, Aakalu VK, Lanahan AA,
946 Sheng M, Worley PF (1999) Coupling of mGluR/Homer and PSD-95 complexes by the
947 Shank family of postsynaptic density proteins. Neuron 23:583-592.
948 Tzakis N, Holahan MR (2019) Social Memory and the Role of the Hippocampal CA2 Region.
949 Front Behav Neurosci 13:233.
950 Walf AA, Frye CA (2007) The use of the elevated plus maze as an assay of anxiety-related
951 behavior in rodents. Nat Protoc 2:322-328.
952 Wang J, Ben Hamida S, Darcq E, Zhu W, Gibb SL, Lanfranco MF, Carnicella S, Ron D (2012)
953 Ethanol-mediated facilitation of AMPA receptor function in the dorsomedial striatum:
954 implications for alcohol drinking behavior. J Neurosci 32:15124-15132.
955 Wang X, Zhan Y (2022) Regulation of Social Recognition Memory in the Hippocampal Circuits.
956 Front Neural Circuits 16:839931.
957 Wei X, Wang J, Yang E, Zhang Y, Qian Q, Li X, Huang F, Sun B (2024) Efr3b is essential for
958 social recognition by modulating the excitability of CA2 pyramidal neurons. Proc Natl Acad
959 Sci U S A 121:e2314557121.
960 Wendholt D, Spilker C, Schmitt A, Dolnik A, Smalla KH, Proepper C, Bockmann J, Sobue K,
961 Gundelfinger ED, Kreutz MR, Boeckers TM (2006) ProSAP-interacting protein 1
962 (ProSAPiP1), a novel protein of the postsynaptic density that links the spine-associated
963 Rap-Gap (SPAR) to the scaffolding protein ProSAP2/Shank3. J Biol Chem 281:13805-
964 13816.
965 Won S, Incontro S, Nicoll RA, Roche KW (2016) PSD-95 stabilizes NMDA receptors by inducing
966 the degradation of STEP61. Proc Natl Acad Sci U S A 113:E4736-4744.

967 Yang X, Gong R, Qin L, Bao Y, Fu Y, Gao S, Yang H, Ni J, Yuan TF, Lu W (2022) Trafficking of
968 NMDA receptors is essential for hippocampal synaptic plasticity and memory
969 consolidation. Cell Rep 40:111217.
970 Zhang H, Etherington LA, Hafner AS, Belelli D, Coussen F, Delagrange P, Chaouloff F, Spedding
971 M, Lambert JJ, Choquet D, Groc L (2013) Regulation of AMPA receptor surface trafficking
972 and synaptic plasticity by a cognitive enhancer and antidepressant molecule. Mol
973 Psychiatry 18:471-484.
974 Zucker RS, Regehr WG (2002) Short-term synaptic plasticity. Annu Rev Physiol 64:355-405.

975

976

977 **Figure 1. Generation and characterization of Prosapip1(flx/flx) mice**

978 **(A)** Identification of guide RNA binding sites in intron 2 and the 3' UTR of exon 5 of Prosapip1.
979 **(B)** PAGE purified Ultramer single stranded DNA oligos that were homologous to the target loci
980 in intron 2 and exon 5 were used as repair templates. **(C)** Genetic crossing scheme of the
981 Prosapip1(flx/flx);Syn1-Cre mice. Male Prosapip1(flx/flx);Syn1-Cre(-/-) mice were mated with
982 female Prosapip1(flx/flx);Syn1-Cre(+/-) mice, leading to litters of Prosapip1(flx/flx);Syn1-Cre(-/-)
983 or Prosapip1(flx/flx);Syn1-Cre(+/-) mice. **(D)** The dHP of C57BL/6, Prosapip1(flx/flx);Syn1-Cre(-)
984 and Prosapip1(flx/flx);Syn1-Cre(+) mice was dissected. Prosapip1 was detected using anti-
985 Prosapip1 antibodies. GAPDH was used as a loading control. **(E)** Histogram of litter size from
986 Prosapip1 mating pairs. X axis depicts number of pups per litter, while Y axis depicts numbers of
987 litters at that size. **(F)** Proportion of male and female offspring from Prosapip1 matings. **(G)**
988 Proportion of Cre(-) and Cre(+) offspring from Prosapip1 matings. **(H)** Body weight of male and
989 female Prosapip1(flx/flx);Syn1-Cre(-) and Prosapip1(flx/flx);Syn1-Cre(+) mice was measured
990 biweekly from birth to assess overt developmental deficits. Data are represented as mean±SEM
991 and analyzed using three-way ANOVA (**Table 1**). n = 10 (Prosapip1(flx/flx);Syn1-Cre(-) male), 5
992 (Prosapip1(flx/flx);Syn1-Cre(-) female), 11 (Prosapip1(flx/flx);Syn1-Cre(+) male), 11
993 (Prosapip1(flx/flx);Syn1-Cre(+) female). **(I-J)** Mice were placed in an open field and locomotion
994 was recorded for 20 minutes. Total distance traveled during the open field test **(I)** and time spent
995 in the center of the open field **(J)**. Data represented as mean±SEM and analyzed using an
996 unpaired t-test (**Table 1**). ns, non-significant. n = 22 (Prosapip1(flx/flx);Syn1-Cre(-)), 21
997 (Prosapip1(flx/flx);Syn1-Cre(+)).

998

999

1000

1001

1002 **Figure 2. Prosapip1 is required for synaptic localization of PSD proteins**

1003 **(A)** The levels of Prosapip1 (top), Synapsin (middle), and CREB (bottom) in the dorsal
1004 hippocampus of Prosapip1(flx/flx);Syn1-Cre(-) mice were measured in the total and crude
1005 synaptosomal fraction. **(B-I)** Total levels of SPAR **(B),** Shank3 **(D, F)**, and PSD-95 **(D, H)**
1006 alongside the synaptic levels of SPAR **(C)**, Shank3 **(E, G)**, and PSD-95 **(E, I)** were measured in
1007 the dHP of Prosapip1(flx/flx);Syn1-Cre(-) and Prosapip1(flx/flx);Syn1-Cre(+) mice using western
1008 blot analysis. Protein levels were normalized to GAPDH and presented as a percentage of the
1009 average of the Prosapip1(flx/flx);Syn1-Cre(-) values. Data are represented as mean±SEM and
1010 analyzed using unpaired two-tailed t-test with Welch's correction (**Table 1**). **p<0.01,
1011 ****p<0.0001; ns, non-significant. n = 5 per group (B-G), 9 (Prosapip1(flx/flx);Syn1-Cre(-)) and 10
1012 (Prosapip1(flx/flx);Syn1-Cre(+)) (H-I). **(J-Q)** The total levels of GluN2A **(J, L)**, GluN2B **(J, N)**, and
1013 GluA1 **(J, P)** and the synaptic levels of GluN2A **(K, M)**, GluN2B **(K, O)**, and GluA1 **(K, Q)** were
1014 measured dHP of Prosapip1(flx/flx);Syn1-Cre(-) and Prosapip1(flx/flx);Syn1-Cre(+) mice via
1015 western blot analysis. Protein levels were normalized to GAPDH and presented as a percentage
1016 of the average of the Prosapip1(flx/flx);Syn1-Cre(-) values. Data are represented as mean±SEM
1017 and analyzed using unpaired two-tailed t-test with Welch's correction (**Table 1**). *p<0.05,
1018 **p<0.01, ***p<0.001; ns, non-significant. n = 4 (Prosapip1(flx/flx);Syn1-Cre(-)), 5
1019 (Prosapip1(flx/flx);Syn1-Cre(+)).

1020 **Figure 3. Prosapip1 in the dorsal hippocampus plays a role in NMDA receptor-mediated**
1021 **transmission and long-term potentiation**

1022 **(A)** Location of stimulating and recording electrodes within the hippocampal CA1 region. **(B)**
1023 Sample field excitatory postsynaptic potential (fEPSP) traces recorded before (pre) and after
1024 (post) administering high-frequency stimulation (HFS) (100Hz, 100 pulses every 20 seconds) in
1025 both Prosapip1(flx/flx);Syn1-Cre(-) (Cre(-)) and Prosapip1(flx/flx);Syn1-Cre(+) (Cre(+)) groups.
1026 **(C)** A stable baseline of fEPSPs was established for 10 minutes before application of HFS and
1027 fEPSPs were recorded for 30 minutes after HFS. Time course of fEPSPs before and after HFS.
1028 **(D)** Quantification of average of fEPSP amplitudes measured between 30-40 minutes. Data are
1029 represented as mean±SEM and analyzed using unpaired two-tailed t-test (**Table 1**). **p<0.01. n
1030 = 10 slices from 6 mice (10/6) (Prosapip1(flx/flx);Syn1-Cre(-)) and (9/5) (Prosapip1(flx/flx);Syn1-
1031 Cre(+)). **(E)** Cells were clamped at -65 mV and the bath contained both DNQX and PTX to block
1032 AMPA and GABA mediated responses. Voltage clamp whole cell recordings and representative
1033 electrically evoked NMDA currents in Prosapip1(flx/flx);Syn1-Cre(-) (Cre(-)) and
1034 Prosapip1(flx/flx);Syn1-Cre(+) (Cre(+)) mice at four stimulation intensities (left). Summarized
1035 responses for Prosapip1(flx/flx);Syn1-Cre(-) (Cre(-)) and Prosapip1(flx/flx);Syn1-Cre(+) (Cre(+))
1036 CA1 neurons quantified by average at each stimulating intensity; #p < 0.05 by two-way repeated
1037 measures ANOVA followed by post-hoc Tukey test (Prosapip1(flx/flx);Syn1-Cre(-) vs.
1038 Prosapip1(flx/flx);Syn1-Cre(+)) at the same stimulating intensities, *p<0.05. n = 14/4
1039 (Prosapip1(flx/flx);Syn1-Cre(-)) and 11/4 (Prosapip1(flx/flx);Syn1-Cre(+)). **(F)** Representative
1040 currents evoked in the CA1 neurons after NMDA bath application (20 uM, 30s) in
1041 Prosapip1(flx/flx);Syn1-Cre(-) (Cre(-)) and Prosapip1(flx/flx);Syn1-Cre(+) (Cre(+)) mice (left).
1042 Average of the peak current elicited by each mouse (right). Data are represented as mean±SEM
1043 and analyzed using unpaired two-tailed t-test (**Table 1**). **p<0.01. n = 13/4
1044 (Prosapip1(flx/flx);Syn1-Cre(-)) and 11/4 (Prosapip1(flx/flx);Syn1-Cre(+)). **(G)** In voltage clamp

1045 recordings, 2 electrical stimulations (100 ms separation) were provided to elicit 2 responses in
1046 the CA1 neurons. PPR was calculated as the amplitude of peak 2/amplitude of peak 1.
1047 Representative paired-pulse ratio in Prosapip1(flx/flx);Syn1-Cre(-) (Cre(-)) and
1048 Prosapip1(flx/flx);Syn1-Cre(+) (Cre(+)) mice (left). Average PPR for Prosapip1(flx/flx);
1049 Syn1-Cre(-) (Cre(-)) and Prosapip1(flx/flx);Syn1-Cre(+) (Cre(+)) (right). Data are represented as
1050 mean±SEM and analyzed using unpaired two-tailed t-test (**Table 1**). *$p<0.05$. n = 11/3
1051 (Prosapip1(flx/flx);Syn1-Cre(-)) and 13/4 (Prosapip1(flx/flx);Syn1-Cre(+)).

1052

1053 **Figure 4. Prosapip1 contributes to recognition, social, and spatial memory**

1054 **(A)** Mice underwent the novel object recognition test, where they were first allowed to explore two
1055 similar objects. After 24 hours, one of the familiar objects was replaced by a novel object, and
1056 mice were again allowed to explore and interact with the objects. Time spent interacting with the
1057 familiar and novel object. n = 22 (Prosapip1(flx/flx);Syn1-Cre(-)), 20 (Prosapip1(flx/flx);Syn1-
1058 Cre(+)). **(B-C)** In the novelty T-maze test, mice were allowed to explore two arms of a three-
1059 armed, T-shaped maze. There were 5 training trials separated by a 1-minute inter-trial interval.
1060 During testing, the third "novel" arm was unblocked and allowed to be explored. **(B)** Difference
1061 score (time exploring novel arm – time exploring familiar arm) performance during the novelty T-
1062 maze test. A positive difference score indicates preference for the novel arm of the maze. n = 22
1063 (Prosapip1(flx/flx);Syn1-Cre(-)), 19 (Prosapip1(flx/flx);Syn1-Cre(+)). **(C)** Heat map of group
1064 average time spent in each arm of the T-maze during the test trial. **(D-E)** Mice performed the 3-
1065 chamber social interaction test. Specifically, they were placed in the center chamber of a 3-
1066 chamber apparatus and allowed to freely explore for 15 minutes for two trials. During the first trial,
1067 one chamber was paired with a juvenile interaction partner (social), while the other chamber
1068 contained only the empty interaction cage (empty). During the second trial, one chamber was
1069 paired with the familiar mouse from the first trial (familiar), and the other chamber contained a
1070 novel juvenile interaction partner (novel). **(D)** Time spent in the empty and social-paired chamber
1071 respectively in the first portion of the 3-chamber social interaction test. n = 14
1072 (Prosapip1(flx/flx);Syn1-Cre(-)), 17 (Prosapip1(flx/flx);Syn1-Cre(+)). **(E)** Time spent in the familiar
1073 and novel chamber during the second portion of the 3-chamber social interaction test. n = 14
1074 (Prosapip1(flx/flx);Syn1-Cre(-)), 17 (Prosapip1(flx/flx);Syn1-Cre(+)). **(F-K)** Mice performed the
1075 Barnes maze test, where they were placed in the center of a white plastic platform with 40
1076 uniformly distributed holes around the perimeter, one of which had an exit compartment placed
1077 underneath. The goal of the trial was to escape into the exit compartment. There were 4 training

1078 trials a day over the course of 4 days, separated by an inter-trial interval of 30 minutes. 24 hours
1079 after the last training trial mice were placed back onto the platform but with the exit compartment
1080 removed (probe trial) and allowed to explore for 5 minutes. **(F)** Average distance traveled from
1081 start point to exit during the Barnes maze training trials. n = 9 (Prosapip1(flx/flx);Syn1-Cre(-)), 12
1082 (Prosapip1(flx/flx);Syn1-Cre(+)). **(G)** Primary (filled circles) and secondary (hollow circles) errors
1083 committed during Barnes maze training. Primary errors are an incorrect hole visit and secondary
1084 errors are an incorrect hole revisit. n = 9 (Prosapip1(flx/flx);Syn1-Cre(-)), 12
1085 (Prosapip1(flx/flx);Syn1-Cre(+)). **(H)** The method of searching utilized by each mouse for each
1086 training trial was qualified. Example path to exit from mice exhibiting random, serial, and spatial
1087 search strategies. **(I-J)** Ratio of search strategy utilization by Prosapip1(flx/flx);Syn1-Cre(-) **(I)**
1088 and Prosapip1(flx/flx);Syn1-Cre(+) **(J)** mice during Barnes maze training. **(K-L)** Time spent in
1089 exit-associated quartile during the probe trial and associated heatmaps **(L)**. n = 9
1090 (Prosapip1(flx/flx);Syn1-Cre(-)), 12 (Prosapip1(flx/flx);Syn1-Cre(+)). Data are represented as
1091 mean±SEM and analyzed using two-way ANOVA (A,C,D,E), Welch's t-test (B), three-way ANOVA
1092 (F), or Mann-Whitney test (J) (**Table 1**). *p<0.05, **p<0.01, ***p<0.001, ****p<0.0001.

1093

1094 **Figure 5. Prosapip1 in the dorsal hippocampus contributes to recognition, social, and**
1095 **spatial memory**

1096 **(A)** Images of AAV-GFP and AAV-Cre overexpression in the dHP of Prosapip1(flx/flx) mice.
1097 **(B)** Western blot analysis of Prosapip1 protein level in the dHP in non-infected mice compared to
1098 mice infected with AAV-Cre. **(C-D)** Mice infected with AAV-GFP or AAV-Cre in the dHP were
1099 placed in an open field, and their behavior was recorded for 20 minutes. The total distance
1100 traveled **(C)** and the time spent in the center of the field **(D)** were measured during the test. n =
1101 19 (AAV-GFP), 15 (AAV-Cre). **(E)** Mice infected with AAV-GFP or AAV-Cre in the dHP were
1102 placed on the light side of a light/dark box apparatus and allowed to explore for 10 minutes. Time
1103 spent in the dark and light chamber during the light/dark box test. n = 19 (AAV-GFP), 15 (AAV-
1104 Cre). **(F)** Mice infected with AAV-GFP or AAV-Cre in the dHP underwent the novel object
1105 recognition test. Briefly, they were familiarized with two similar objects before one was switched
1106 for a novel object after 24 hours. Cumulative time spent exploring the familiar and novel object
1107 during the novel object recognition test. n = 16 (AAV-GFP), 17 (AAV-Cre). **(G)** Mice infected with
1108 AAV-GFP or AAV-Cre in the dHP underwent the novelty T-maze test, where they were first
1109 allowed to explore two arms of a three-armed, T-shaped maze. During the testing phase, the third
1110 "novel" arm was unblocked and made available for exploration. Difference score (time exploring
1111 novel arm – time exploring familiar arm) of time spent exploring the novel arm of the T-maze. A
1112 heatmap of each average group performance during the test is also presented. n = 18 (AAV-
1113 GFP), 15 (AAV-Cre). **(H-I)** Mice infected with AAV-GFP or AAV-Cre in the dHP performed the 3-
1114 chamber social interaction test. Briefly, they were placed in the center chamber and allowed to
1115 freely explore for 15 minutes during two trials. In the first trial, one chamber had a juvenile
1116 interaction partner, and the other was empty. In the second trial, one chamber had the familiar
1117 mouse from the first trial, and the other had a new juvenile interaction partner. **(H)** Cumulative
1118 time spent in the empty and social chamber of the 3-chamber social interaction test. n = 18 (AAV-

1119 GFP), 15 (AAV-Cre). **(I)** Cumulative time spent in the familiar and novel chambers in the 3-
1120 chamber social interaction test. n = 18 (AAV-GFP), 15 (AAV-Cre). **(J-K)** Mice infected with AAV-
1121 GFP or AAV-Cre in the dHP underwent the Barnes maze experiment. They were placed in the
1122 center of a platform with 40 evenly spaced holes around the perimeter, one of which led to an exit
1123 compartment. Mice underwent 4 training trials per day for 4 days, with 30-minute intervals
1124 between trials. Twenty-four hours after the last training trial, they were placed back on the platform
1125 without the exit compartment (probe trial) and allowed to explore for 5 minutes. **(J)** Average
1126 distance traveled from start point to exit during the Barnes maze training trials. n = 8 (AAV-GFP),
1127 6 (AAV-Cre). **(K)** Time spent in the exit quartile during the probe trial. n = 8 (AAV-GFP), 6 (AAV-
1128 Cre). Data are represented as mean±SEM and analyzed using two-way ANOVA (E, F, H, I, J),
1129 Welch's t-test (C, D, G), or Mann-Whitney test (K) (**Table 1**). *p<0.05, **p<0.01, ***p<0.001,
1130 ****p<0.0001.

1131

1132 **Extended Figure 4. Prosapip1 knockout did not affect Barnes maze exploratory behavior**
1133 **or baseline anxiety**

1134 **(A)** Before the Barnes maze training trials began, mice were placed on the platform to assess
1135 baseline exploratory behavior and locomotion in the environment. The exit compartment was in a
1136 different location than training trials. Distance traveled during the Barnes maze habituation trial.
1137 Data represented as mean±SEM and analyzed using unpaired t-test (**Table 1**). ns, non-
1138 significant. n = 6 (Prosapip1(flx/flx);Syn1-Cre(-)), 12 Prosapip1(flx/flx);Syn1-Cre(+). **(B)** To assess
1139 anxiety, mice were placed on the light side of a light/dark box apparatus and allowed to explore
1140 for 10 minutes. Time spent in the light and dark chamber during the test. Data represented as
1141 mean±SEM and analyzed using a two-way ANOVA (**Table 1**). ****$p<0.0001$. n = 15
1142 (Prosapip1(flx/flx);Syn1-Cre(-)), 16 (Prosapip1(flx/flx);Syn1-Cre(+)). **(C)** Mice were placed in the
1143 center of a plus-shaped maze and allowed to explore two closed and two open arms for 5 minutes
1144 to assess anxiety and exploratory behavior. Time spent in the open arm of the elevated plus
1145 maze. Open-arm time was measured and analyzed using unpaired two-tailed t-test (**Table 1**). ns,
1146 non-significant. n = 7 (Prosapip1(flx/flx);Syn1-Cre(-)), 17 (Prosapip1(flx/flx);Syn1-Cre(+)).

Figure 1

Generation and characterization of Prosapip1(flx/flx) mice

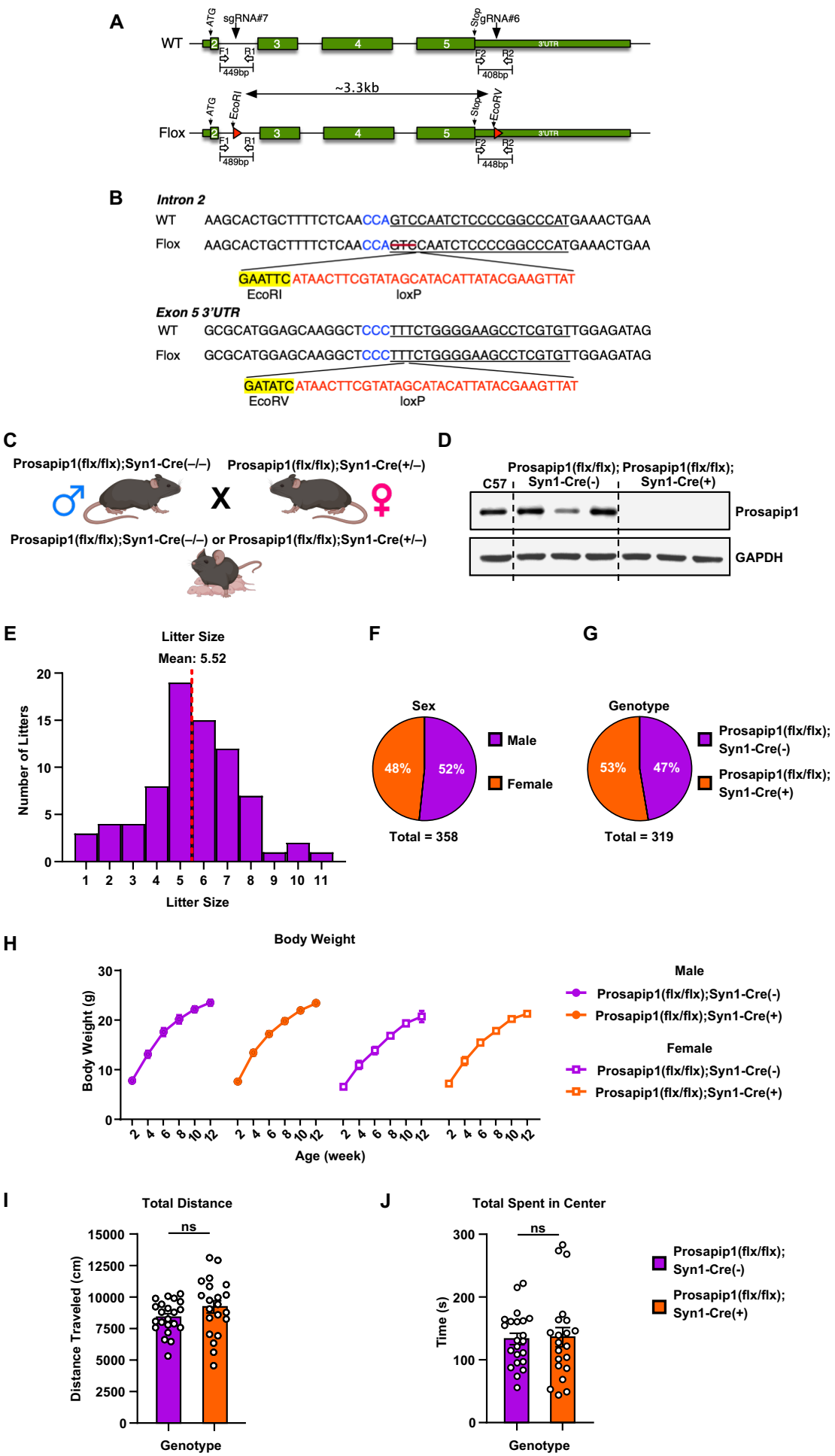

Figure 2

Prosapip1 is required for synaptic localization of PSD proteins

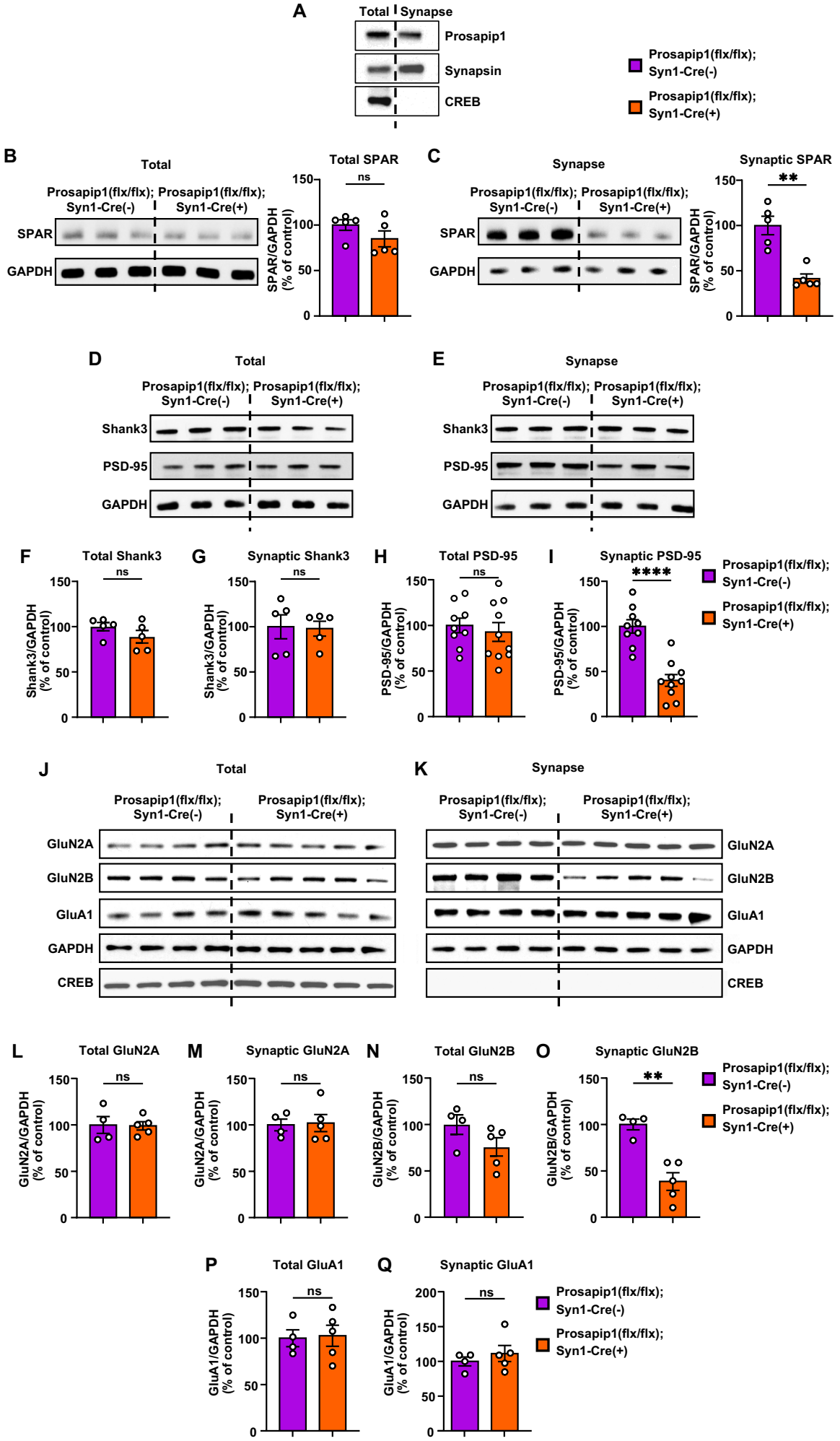

Figure 3

Prosapip1 in the dorsal hippocampus plays a role in NMDA receptor-mediated transmission and long-term potentiation

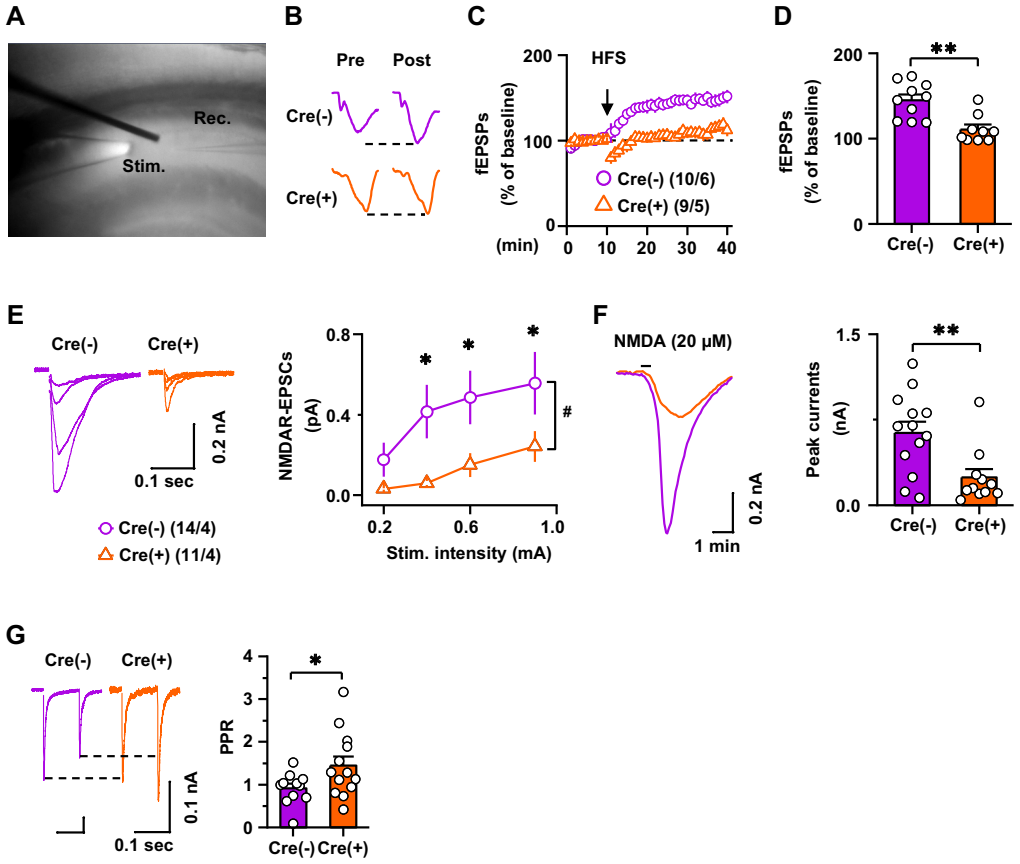

Figure 4

Prosapip1 contributes to recognition, social, and spatial memory

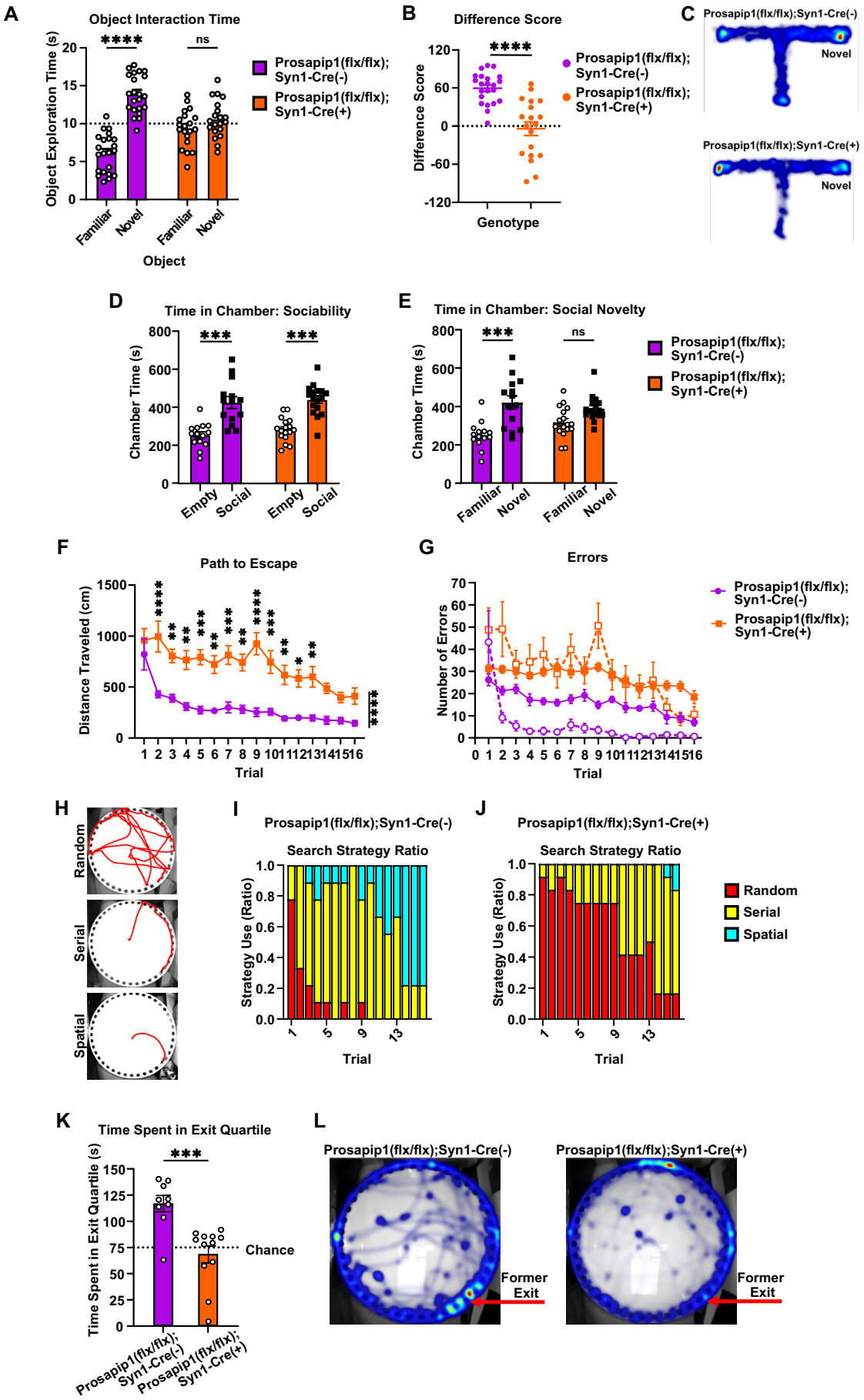

Figure 5

Prosapip1 in the dorsal hippocampus contributes to recognition, social, and spatial memory

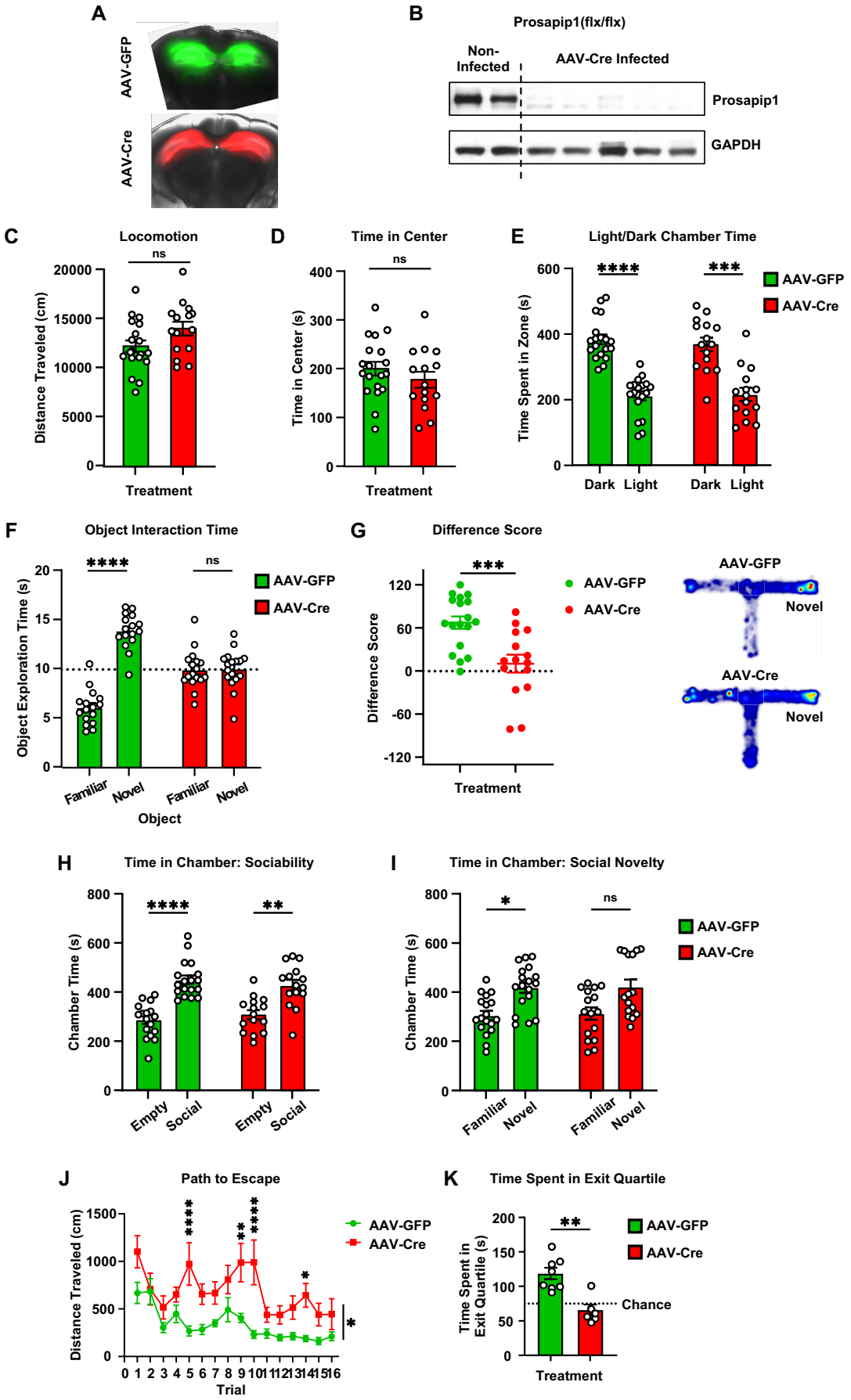

Extended Figure 4

Prosapip1 knockout did not affect Barnes maze exploratory behavior or baseline anxiety

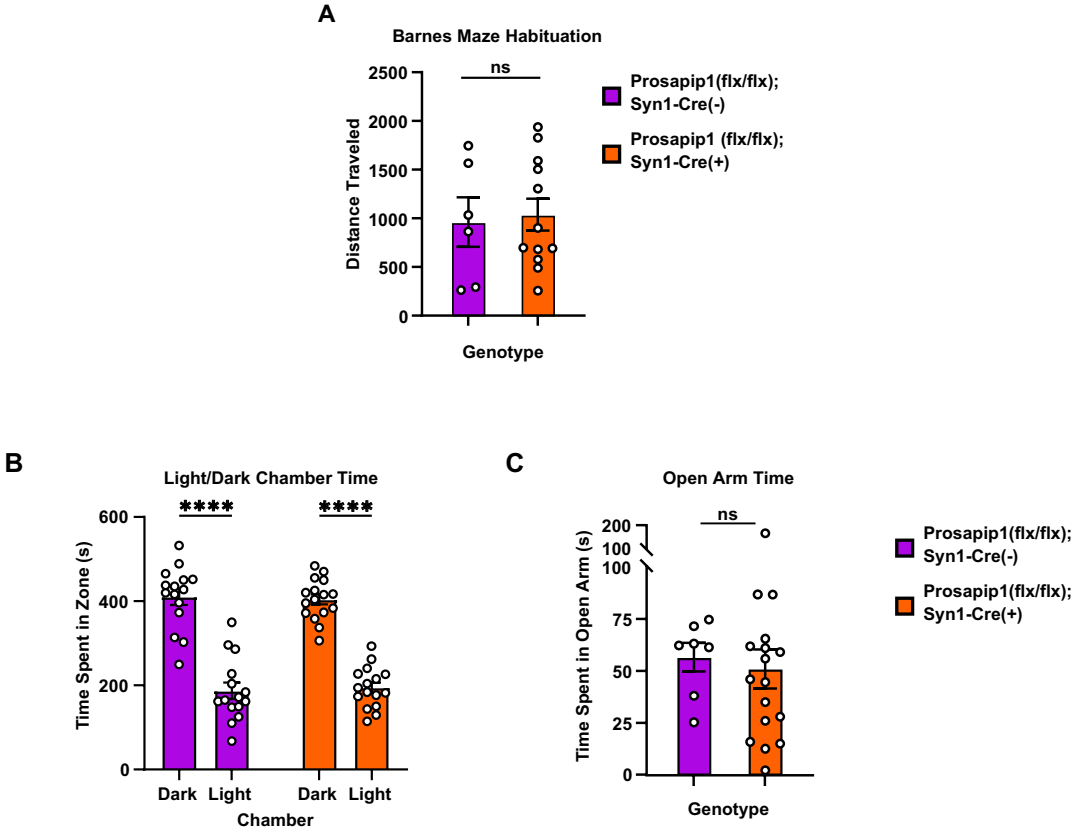

Table 1. Statistics

Figure	n	Sex Difference	Statistical Test	Effect	Result	p-value	Post-hoc	Post-hoc comparison	p-value
1E	77		D'Agostino & Pearson	Normality	K2 = 5.480	0.0646			
1H	10 (Cre- Male), 5 (Cre- Female), 11 (Cre+ Male), 11 (Cre+ Female)	Yes	Three-way ANOVA	Genotype	$F_{(1,33)}$ = 0.7842	0.3823			
				Sex	$F_{(1,33)}$ = 23.94	< 0.0001			
				Time	$F_{(5,158)}$ = 588.4	< 0.0001			
				Genotype x Sex	$F_{(1,33)}$ = 1.345	0.2545			
				Genotype x Time	$F_{(5,158)}$ = 0.1476	0.9805			
				Sex x Time	$F_{(5,158)}$ = 2.345	0.0437			
				Genotype x Sex x Time	$F_{(5,158)}$ = 0.3764	0.8643			
1I	22 (Cre-), 21 (Cre+)	No	Unpaired t-test	Genotype	$t_{(41)}$ = 1.460	0.1518			
1J	22 (Cre-), 21 (Cre+)	No	Mann-Whitney Test	Genotype	U = 220	0.8007			
2B	5 (Cre-), 5 (Cre+)		Unpaired t-test	Genotype	$t_{(6.963)}$ = 1.427	0.1968			
2C	5 (Cre-), 5 (Cre+)		Unpaired t-test	Genotype	$t_{(5.880)}$ = 5.183	0.0022			
2F	5 (Cre-), 5 (Cre+)		Unpaired t-test	Genotype	$t_{(6.932)}$ = 1.345	0.221			
2G	5 (Cre-), 5 (Cre+)		Unpaired t-test	Genotype	$t_{(6.720)}$ = 0.1306	0.8999			
2H	9 (Cre-), 10 (Cre+)		Unpaired t-test	Genotype	$t_{(16.38)}$ = 0.5588	0.5839			
2I	9 (Cre-), 10 (Cre+)		Unpaired t-test	Genotype	$t_{(16.44)}$ = 6.095	< 0.0001			
2L	4 (Cre-), 5 (Cre+)		Unpaired t-test	Genotype	$t_{(4.429)}$ = 0.1050	0.921			
2M	4 (Cre-), 5 (Cre+)		Unpaired t-test	Genotype	$t_{(6.689)}$ = 0.1758	0.8656			
2N	4 (Cre-), 5 (Cre+)		Unpaired t-test	Genotype	$t_{(6.700)}$ = 1.675	0.1398			
2O	4 (Cre-), 5 (Cre+)		Unpaired t-test	Genotype	$t_{(6.332)}$ = 5.524	0.0012			
2P	4 (Cre-), 5 (Cre+)		Unpaired t-test	Genotype	$t_{(6.956)}$ = 0.1831	0.8599			
2Q	4 (Cre-), 5 (Cre+)		Unpaired t-test	Genotype	$t_{(6.060)}$ = 0.8548	0.4252			
3D	10/6 (Cre-), 9/5 (Cre+)		Unpaired t-test	Genotype	$t_{(17)}$ = 3.933	0.0011			
3E	14/4 (Cre-), 11/4 (Cre+)		Two-way ANOVA	Genotype	$F_{(1,3)}$ = 9.441	0.044	Tukey	0.2 (Cre- vs. Cre+)	0.345
				Intensity	$F_{(1,3)}$ = 9.441	< 0.001		0.4 (Cre- vs. Cre+)	0.025
				Genotype x Intensity	$F_{(1,3)}$ = 1.376	0.258		0.6 (Cre- vs. Cre+)	0.034
								0.9 (Cre- vs. Cre+)	0.046
3F	3/4 (Cre-), 11/4 (Cre+)		Unpaired t-test	Genotype	$t_{(22)}$ = 3.094	0.00529			
3G	11/3 (Cre-), 13/4 (Cre+)		Unpaired t-test	Genotype	$t_{(22)}$ = 2.099	0.0475			
4A	22 (Cre-), 20 (Cre+)	No	Two-way ANOVA	Genotype	$F_{(1,40)}$ = 0.3079	= 0.5821	Šidák	Familiar vs. Novel (Cre-)	<0.0001
				Object	$F_{(1,40)}$ = 34.32	< 0.0001		Familiar vs. Novel (Cre+)	0.4871
				Genotype x Object	$F_{(1,40)}$ = 18.37	0.0001			
4B	22 (Cre-), 19 (Cre+)	No	Unpaired t-test	Genotype	$t_{(26.08)}$ = 5.434	< 0.0001			
4D	14 (Cre-), 17 (Cre+)	No	Two-way ANOVA	Genotype	$F_{(1,29)}$ = 5.419	0.0271	Šidák	Empty vs. Social (Cre-)	0.0006
				Social	$F_{(1,29)}$ = 34.30	< 0.0001		Empty vs. Social (Cre+)	0.0005
				Genotype x Social	$F_{(1,29)}$ = 0.05655	0.8137			
4E	14 (Cre-), 17 (Cre+)	No	Two-way ANOVA	Genotype	$F_{(1,29)}$ = 1.463	0.2362	Šidák	Familiar vs. Novel (Cre-)	0.0008
				Social Novelty	$F_{(1,29)}$ = 17.60	0.0002		Familiar vs. Novel (Cre+)	0.1451
				Genotype x Social Novelty	$F_{(1,29)}$ = 2.947	0.0967			
Ext. 4A	6 (Cre-), 12 (Cre+)	No	Unpaired t-test	Genotype	$t_{(16)}$ = 0.2635	0.7955			
4F	9 (Cre-), 12 (Cre+)	No	Two-way ANOVA	Genotype	$F_{(1,19)}$ = 102.0	< 0.0001	Šidák	Trial 2 (Cre- vs. Cre+)	<0.0001
				Trial	$F_{(15,285)}$ = 7.899	< 0.0001		Trial 3 (Cre- vs. Cre+)	0.0067
				Genotype x Trial	$F_{(15,285)}$ = 1.401	0.1454		Trial 4 (Cre- vs. Cre+)	0.0018
								Trial 5 (Cre- vs. Cre+)	0.0002
								Trial 6 (Cre- vs. Cre+)	0.002
								Trial 7 (Cre- vs. Cre+)	0.0002
								Trial 8 (Cre- vs. Cre+)	0.0016
								Trial 9 (Cre- vs. Cre+)	<0.0001
								Trial 10 (Cre- vs. Cre+)	0.0006
								Trial 11 (Cre- vs. Cre+)	0.0049
								Trial 12 (Cre- vs. Cre+)	0.0169
								Trial 13 (Cre- vs. Cre+)	0.0098
4G	9 (Cre-), 12 (Cre+)	No	Three-way ANOVA	Genotype	$F_{(1,19)}$ = 100.7	< 0.0001			
				Trial	$F_{(15,289)}$ = 7.289	< 0.0001			
				Error Type	$F_{(0.4468, 8.489)}$ = 4.55	0.0772			
				Genotype x Trial	$F_{(15,289)}$ =1.529	0.094			
				Genotype x Error Type	$F_{(1,19)}$ = 15.09	0.001			
				Trial x Error Type	$F_{(6.157, 117)}$ = 2.865	0.0115			
				Genotype x Trial x Error Type	$F_{(15,285)}$ = 1.831	0.0303			
4K	9 (Cre-), 12 (Cre+)	No	Mann-Whitney Test	Genotype	U = 8	0.0004			
Ext. 4B	15 (Cre-), 16 (Cre+)	No	Two-way ANOVA	Chamber	$F_{(1,29)}$ = 92.69	< 0.0001	Šidák	Light vs. Dark (Cre-)	<0.0001
				Genotype	$F_{(1,29)}$ = 0.9504	0.3377		Light vs. Dark (Cre+)	<0.0001
				Genotype x Chamber	$F_{(1,29)}$ = 0.09645	0.7584			
Ext. 4C	7 (Cre-), 17 (Cre+)	No	Mann-Whitney Test	Genotype	U = 42	0.2878			
5C	19 (AAV-GFP), 15 (AAV-Cre)	No	Unpaired t-test	Treatment	$t_{(29.59)}$ = 1.961	0.0594			
5D	19 (AAV-GFP), 15 (AAV-Cre)	No	Unpaired t-test	Treatment	$t_{(29.72)}$ = 1.066	0.2951			
5E	19 (AAV-GFP), 15 (AAV-Cre)	No	Two-way ANOVA	Treatment	$F_{(1,32)}$ = 2.361	0.1342	Šidák	Light vs. Dark (AAV-GFP)	<0.0001
				Chamber	$F_{(1,32)}$ = 46.74	< 0.0001		Light vs. Dark (AAV-Cre)	0.0003
				Treatment x Chamber	$F_{(1,32)}$ = 0.1588	0.6929			
5F	16 (AAV-GFP), 17 (AAV-Cre)	No	Two-way ANOVA	Treatment	$F_{(1,31)}$ = 3.069	0.0897	Šidák	Familiar vs. Novel (AAV-GFP)	< 0.0001
				Object	$F_{(1,31)}$ = 36.30	< 0.0001		Familiar vs. Novel (AAV-Cre)	0.9965
				Treatment x Object	$F_{(1,31)}$ = 35.05	< 0.0001			
5G	18 (AAV-GFP), 15 (AAV-Cre)	No	Unpaired t-test	Treatment	$t_{(26.04)}$ = 3.777	0.0008			
5H	18 (AAV-GFP), 15 (AAV-Cre)	No	Two-way ANOVA	Treatment	$F_{(1,31)}$ = 0.0003957	0.9843	Šidák	Empty vs. Social (AAV-GFP)	<0.0001
				Social	$F_{(1,31)}$ = 31.60	< 0.0001		Empty vs. Social (AAV-Cre)	0.0062
				Treatment x Social	$F_{(1,31)}$ = 0.7781	0.3845			
5I	18 (AAV-GFP), 15 (AAV-Cre)	No	Two-way ANOVA	Treatment	$F_{(1,31)}$ = 0.2045	0.6543	Šidák	Familiar vs. Novel (AAV-GFP)	0.0303
				Social Novelty	$F_{(1,31)}$ = 9.777	0.0038		Familiar vs. Novel (AAV-Cre)	0.1319
				Treatment x Social Novelty	$F_{(1,31)}$ = 0.1131	0.7389			
5J	8 (AAV-GFP), 6 (AAV-Cre)	No	Two-way ANOVA	Treatment	$F_{(1,12)}$ = 22.95	0.0004	Šidák	Trial 5 (AAV-GFP vs. AAV-Cre)	<0.0001
				Trial	$F_{(15,180)}$ = 6.246	< 0.0001		Trial 9 (AAV-GFP vs. AAV-Cre)	0.0026
				Treatment x Trial	$F_{(15,180)}$ = 2.033	0.0153		Trial 10 (AAV-GFP vs. AAV-Cre)	<0.0001
								Trial 14 (AAV-GFP vs. AAV-Cre)	0.0475
5K	8 (AAV-GFP), 6 (AAV-Cre)	No	Mann-Whitney Test	Treatment	U = 3	0.0047			